Cardiac MRI at Low Field Strengths

Adrienne E. Campbell-Washburn, PhD,[1*] Juliet Varghese, PhD,[2] Krishna S. Nayak, PhD,[3,4] Rajiv Ramasawmy, PhD,[1] and Orlando P. Simonetti, PhD[5,6]

Cardiac MR imaging is well established for assessment of cardiovascular structure and function, myocardial scar, quantitative flow, parametric mapping, and myocardial perfusion. Despite the clear evidence supporting the use of cardiac MRI for a wide range of indications, it is underutilized clinically. Recent developments in low-field MRI technology, including modern data acquisition and image reconstruction methods, are enabling high-quality low-field imaging that may improve the cost–benefit ratio for cardiac MRI. Studies to-date confirm that low-field MRI offers high measurement concordance and consistent interpretation with clinical imaging for several routine sequences. Moreover, low-field MRI may enable specific new clinical opportunities for cardiac imaging such as imaging near metal implants, MRI-guided interventions, combined cardiopulmonary assessment, and imaging of patients with severe obesity. In this review, we discuss the recent progress in low-field cardiac MRI with a focus on technical developments and early clinical validation studies.
Evidence Level: 5
Technical Efficacy: Stage 1

J. MAGN. RESON. IMAGING 2024;59:412–430.

Over the past three decades, significant technical advances and rigorous clinical validation have established cardiovascular magnetic resonance imaging as the gold standard for the assessment of cardiovascular structure and function and myocardial scar.[1] Cardiac MRI is technically demanding, requiring rapid imaging to resolve cardiac motion or to "freeze" a specific cardiac phase. Advances in MRI pulse sequences, reconstruction methods, and image processing have improved reliability and efficiency, and broadened clinical applications.

Cardiac MRI is the modality of choice for evaluation of the right ventricle,[2] and velocity encoded MRI is important in the assessment of valvular disease and congenital heart disease.[3] Cardiac MRI also offers unique methods to characterize myocardial tissue by a variety of mechanisms not provided by other cardiac imaging modalities. Late gadolinium enhancement (LGE) identifies myocardial injury or replacement fibrosis,[4] which can uniquely determine the etiology of heart failure and a variety of cardiomyopathies and is highly prognostic for risk of arrhythmias or sudden cardiac death. More recently, myocardial T1 and T2 relaxation parameter mapping and extracellular volume (ECV) fraction mapping have been used to identify myocardial interstitial expansion and edema/inflammation, and these measures have proven to have significant diagnostic and prognostic value.[5–7] Furthermore, there is a growing body of evidence supporting the advantages of first-pass perfusion MRI with vasodilator stress for the evaluation of ischemic heart disease.[8,9] The data supporting the diagnostic and prognostic effectiveness of cardiac MRI has led to expanded inclusion in a number of guidelines on the recommended use of cardiac imaging put forth by the European Society of Cardiology and the American College of Cardiology/American Heart Association.[10–12]

Despite the clear evidence supporting the clinical utilization of cardiac MRI for a wide range of indications, it is not commonly used outside of large, urban, academic medical centers in high-income countries. Several factors have prevented its widespread adoption.[13] Relative to widely utilized neurological

View this article online at wileyonlinelibrary.com. DOI: 10.1002/jmri.28890

Received Mar 17, 2023, Accepted for publication Jun 16, 2023.

*Address reprint requests to: A.E.C.-W., 10 Center Dr., Building 10 Rm B1D219, Bethesda, MD 20892, USA.
E-mail: adrienne.campbell@nih.gov

From the [1]Cardiovascular Branch, National Heart, Lung, and Blood Institute, National Institutes of Health, Bethesda, Maryland, USA; [2]Department of Biomedical Engineering, The Ohio State University, Columbus, Ohio, USA; [3]Ming Hsieh Department of Electrical and Computer Engineering, Viterbi School of Engineering, University of Southern California, Los Angeles, California, USA; [4]Alfred Mann Department of Biomedical Engineering, Viterbi School of Engineering, University of Southern California, Los Angeles, California, USA; [5]Division of Cardiovascular Medicine, Department of Internal Medicine, College of Medicine, The Ohio State University, Columbus, Ohio, USA; and [6]Department of Radiology, The Ohio State University, Columbus, Ohio, USA

Additional supporting information may be found in the online version of this article

and musculoskeletal MRI, cardiac MRI exams tend to be complicated to perform, and require technologists and physicians with a high level of specialized expertise. The time-consuming nature of cardiac MRI makes it challenging to justify in environments where MRI resources are limited. In the United States in particular, this challenge is compounded by the fact that cardiac MRI reimbursement rates are unfavorable relative to echocardiography and single photon emission tomography (SPECT), despite the significantly higher costs to purchase, install, maintain, and operate an MRI scanner compared to these other cardiac imaging modalities.[14] Additionally, compared to echocardiography and cardiac SPECT, MRI poses greater challenges for severely obese and claustrophobic patients, those unable to breath-hold repeatedly, and for the growing number of patients with cardiac implanted electronic devices (CIED). These factors and others have limited cardiac MRI utilization in the United States to represent only a small fraction of all MRI scans performed (<5%), and an even smaller fraction of cardiac imaging performed using all modalities (<3%).

Recent developments in low-field MRI technology have opened new opportunities to address some of the challenges impeding widespread utilization of cardiac MRI by favorably shifting the cost–benefit ratio for MRI in terms of reduced purchase, installation, and maintenance costs, and potential for reduced operational complexity.[15–17] There is growing evidence that routine cardiac MRI can be performed on contemporary low-field MRI systems with gradient and receiver coil hardware suitable for the technical demands of cardiac imaging.[15,18–20] Additionally, modern data acquisition and model-based or machine learning driven image reconstruction methods are becoming more widely available and further enable low-field MRI. In addition to cost-savings, low-field MRI offers several other potential benefits, for example in patients with implants, for MRI-guided interventional procedures, for examining cardiopulmonary interactions, and for obese patients. Moreover, the deployment of low-field MRI directly in patient care environments such as cardiology, intensive care, emergency departments, and community-based centers may be achievable. The opportunities and challenges of low-field cardiac MRI are outlined in Table 1.

Low-field cardiac MRI is actively under development, with the common goal to expand the availability of imaging to patient groups and underserved geographical regions with limited access to MRI, and to develop applications that are better suited to low field. This article will review the current state of low-field cardiac MRI, defined here as <1.0 T, with a focus on recent and emerging technical developments and early clinical validation studies.

History of Low Field Cardiac MRI

Beginning in the early 1980s, the first commercial MRI units operated at field strengths <0.5 T. Cardiac imaging was attempted very early on, with the first description of clinical cardiac MRI published in 1983[21] using a 0.35 T system (Oxford Instruments). Gated and ungated spin echo imaging was used in 244 subjects, and clear delineation of cardiac chambers and pathologies of the aorta including dissection, aneurysm, and atheroma were reported.

The magnetic field strength (B0) used for clinical MRI immediately started on an upward trajectory, with the first 1.5 T commercial system introduced by General Electric in 1983. By the 1990's, 1.5 T quickly became the clinical standard and dominated the MRI market. Over the next two decades, the pursuit of higher signal-to-noise ratio (SNR) and increased image resolution drove B0 to 3.0 T and higher. While high-field magnets have proven beneficial for many neurological and musculoskeletal imaging applications, there have been no clear direct benefits for most cardiac imaging applications. In addition, higher B0 brings increased system cost, safety concerns, image artifacts, and restrictions on magnet configuration. As such, 1.5 T remains the predominant field strength for cardiac MRI.

While lower field units remained on the market during this period, these were viewed as inferior to high-field MRI and were marketed primarily for their lower cost and "open" bore configuration. Minor efforts have been ongoing to explore the potential for cardiac imaging on the existing low-field scanners. Even though these low-field systems were equipped with reduced performance gradient and RF systems, reasonable cardiac and vascular imaging across a range of applications at fields <1.5 T have been demonstrated.[22–25] For example, a 0.5 T system (Surrey Medical Imaging Systems Ltd., Surrey, U.K.) was used to demonstrate first-pass perfusion and for cardiac imaging in patients with pacemakers[26,27]; a 0.5 T double-donut interventional MRI system (GE Signa SP, GE Medical Systems, Milwaukee, WI, USA) was used for upright exercise stress during flow quantification[28]; an open 0.7 T system (Altaire, Hitachi Medical Corporation) was used for cine imaging with parallel imaging[23]; an open 0.35 T system (MAGNETOM C!, Siemens Healthcare, Erlangen, Germany) was used for cine, perfusion and late enhancement on a cohort of patients[22]; and a 0.2 T system (Signa Profile version 7.6; GE-Yokogawa Medical Systems, Tokyo, Japan) was used to develop interventional device tracking techniques.[29]

Along with the move to 1.5 T and 3 T fields in the 1990's and early 2000's, respectively, there have been concurrent advances in RF and gradient systems. Until recently, these advances have not been combined with lower field strength magnets. Contemporary clinical gradient systems have maximum amplitude and slew rates in the range of 45 mT/m and 200 T/m/s respectively, facilitating the implementation of short repetition (TR) and echo times (TE) that are critical for cardiac pulse sequences. Advances in multi-channel receiver coil design have facilitated the development of parallel imaging acceleration

TABLE 1. Opportunities and Challenges for Cardiac MRI at Low Field, compared to 1.5T or 3T.

Opportunities		Challenges	
Opportunity	**Implications**	**Challenge**	**Possible Solutions**
Reduced system cost	• Increased availability in previously underserved areas • Increase usage in healthcare systems with unfavorable reimbursement	Perception that low field = low quality	• Validation studies demonstrating high quality diagnostic cardiac MRI at low field
Reduced siting requirements	• Installation directly in patient care environments (cardiology, ICU, emergency room, etc.)	Lower SNR	• SNR efficient acquisitions leveraging long signal readouts (long T2*), short T1, and high flip angles • Advanced image reconstruction and processing
Improved patient comfort and monitoring	• Wide-bore systems for imaging obese or claustrophobic patients • Higher quality ECG due to reduced MHD effect • Reduced acoustic noise	Low acceleration rates	• Receiver coil array design and optimization • Advanced image reconstruction
Low susceptibility	• Reduced artifacts from implants • Improved pulmonary imaging to enable cardiopulmonary exams • Sequence design flexibility	Concomitant field artifacts	• Sequence- and reconstruction-based mitigation and correction
Low SAR	• MRI guided interventional procedures using metallic devices • Improved safety of some implants and CIEDs • Sequence design flexibility	Lack of regulatory approval for implanted devices	• Research demonstrating device safety

techniques that were instrumental in the application of rapid, segmented k-space, breath-held imaging, and single-shot/real-time free-breathing cardiac imaging techniques. GeneRalized Autocalibrating Partial Parallel Acquisition (GRAPPA) and Sensitivity Encoding (SENSE)-based parallel imaging techniques are routinely used in cardiac MRI to reconstruct under-sampled data, although these methods incur an SNR penalty that is not always compatible with low field. In the past decade, compressed sensing (CS) inspired recovery methods, and more recently machine learning-based methods, have altered the traditional trade-offs between scan time and SNR, opening the possibility for high quality routine and advanced cardiac imaging techniques at low field.

Over the past 6 years, cardiac applications have been explored by several research groups using both commercial and prototype whole-body low-field systems equipped with superconducting magnets, contemporary hardware, and contemporary software; these systems are summarized in Table 2. Two higher field commercial scanners have been ramped down to use a unique combination of lower main magnetic field (0.55 T and 0.75 T) with high performance gradient and RF systems.[16,30] Commercially available low-field systems with demonstrated cardiac imaging capabilities include the 0.35 T ViewRay MRIdian (ViewRay Inc. Oakwood, USA), and the 0.55 T Siemens MAGNETOM Free.Max (Siemens Healthcare, Erlangen, Germany). This Siemens system is considerably lighter in weight (~3.2 tons) than higher field magnets, and uses very little helium (<1 liter), eliminating the need for a quench pipe and reducing site preparation, installation, and maintenance costs.[17,31]

Low Field Imaging Properties and Imaging Technology

Favorable Imaging Properties

MRI at field strengths <1 T provides many favorable properties for cardiac imaging. As briefly described in this section,

TABLE 2. Contemporary Low Field Strength MRI Systems That Have Demonstrated Cardiac MRI

Field Strength	System	System Type	Gradient Specifications	Bore Diameter (cm)
0.35 T	MRIdian, ViewRay Inc. Oakwood, USA	Commercial MR-linac system for MR-guided radiotherapy with split bore	18 mT/m, 200 T/m/msec	70
0.55 T	MAGNETOM Aera, Siemens Healthcare, Erlangen, German	Prototype ramped-down from 1.5 T with custom transmit/receive body coil	45 mT/m, 200 T/m/msec	70
0.55 T	MAGNETOM Free.Max, Siemens Healthcare, Erlangen, Germany	Commercial whole-body MRI	26 mT/m, 45 T/m/s	80
0.75 T	Achieva, Philips Healthcare, Best, The Netherlands	Prototype ramped-down from 3 T using 13C components and multi-nuclear broadband spectrometer/coils	31 mT/m, 200 T/m/s	60

these include simplified cardiac gating, reduced artifacts around implant hardware, and improved patient comfort.

CARDIAC GATING. Most cardiac MRI methods rely on synchronization with the cardiac cycle using in-bore electrocardiography (ECG) or photo plethysmography. ECG is preferred because triggering on the sharp and high-amplitude R-wave enables prospective capturing of systolic contraction. ECG signals obtained at lower B0 field strengths are less noisy and more reliable, primarily due to the reduced magnetohydrodynamic (MHD) effect that is proportional to B0. However, ECG signals may still be susceptible to interference from RF and imaging gradients across field strengths. At higher field strengths such as 3 T, the MHD artifact is a significant source of mis-gating, requiring more sophisticated multi-channel solutions like vector-cardiogram gating.[32] Low-field imaging can thus provide reliable cardiac ECG gating with reduced complexity and cost. Figure 1 contains illustrative ECG samples from 0.75 T to 1.5 T.

IMPLANT ARTIFACTS. Metallic implants are extremely common in cardiac patients, and include sternal wires, stents, valve clips, prosthetic valves, occlusion devices, and CIEDs. The increasing prevalence of these implants has created a growing patient population in whom cardiac MRI can be extremely challenging or infeasible. Although MRI safety in patients with CIEDs has now been well documented,[34–36] cardiac MRI of patients with CIEDs can be challenging due to metal-induced image artifacts.[37,38] The presence of these foreign metals disturbs the homogeneity of the B0 field, producing significant

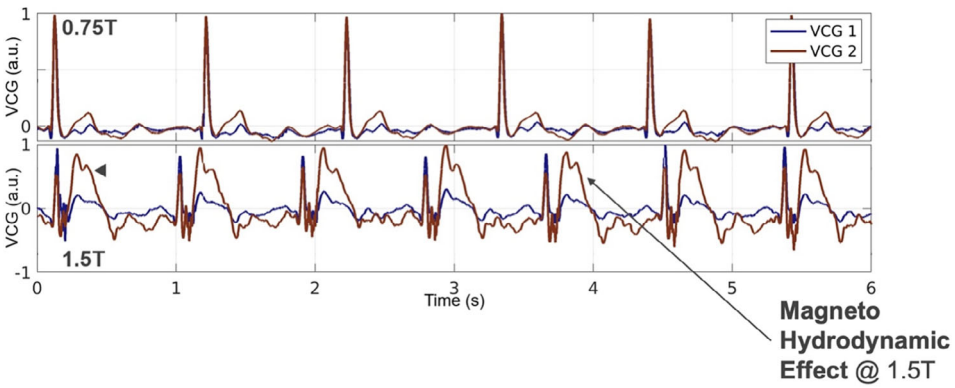

FIGURE 1: Illustration of the reduced magnetohydrodynamic (MHD) effect at 0.75 T (top) compared to 1.5 T (bottom). This MHD effect can be resolved using vector gating, with additional leads and higher complexity of the gating system. In general, low field strengths enable simpler and more robust ECG gating with a single channel. [Reproduced from Guenther et al.[30]]

artifacts.[39] As the degree of signal distortion is proportional to B0, all artifacts (signal loss, banding, spatial distortions) are dramatically reduced at lower field strengths. In short, low-field imaging is expected to provide improved quality near the metallic hardware site (see "*Advanced Applications*" section). Moreover, RF-induced heating scales quadratically with B0, and additionally depends on the coupling between the RF field and conductor device to form standing waves. At low field, the RF wavelength is longer, potentially preventing coupling with short conductive leads. Therefore, low-field MRI possibly allows for safer imaging in patients with broken or abandoned leads, which remain a contraindication to MRI due to the risk of heating.[40]

PATIENT COMFORT. Two of the most frequent MRI subject complaints are acoustic noise, and claustrophobia, both of which can be reduced at low field.[41] Acoustic noise (and system vibration) is generated by vibration of the gradient coil when the gradient changes (dG/dt) in the presence of the static field (B0). It is, therefore, proportional to both dG/dt and B0. The noise a patient hears and the vibration they feel is also highly dependent on the mechanical engineering of the entire system, which includes sophisticated vibration dampening. However, with all else constant, the acoustic noise from an MRI sequence is indeed linear with B0, meaning that low field reduces acoustic noise.[42] Regarding claustrophobia, lower B0 changes the constraints on the superconducting magnet design, which makes it feasible to produce wider bore low-field systems. This reduces claustrophobia, and improves overall comfort for larger subjects, including patients who are obese or pregnant.

Image Contrast

Endogenous NMR relaxation parameters vary with field strength.[43] Generally, at low field, T1 relaxation times are shorter, and T2 and T2* relaxation times are longer. Table 3 provides reported T1, T2, and T2* values from 0.35 T to 0.55 T compared to 1.5 T and 3 T for myocardium and blood.[16,31] For cardiac imaging, the shorter T1 relaxation times result in more signal recovery during rapid imaging sequences that have short TR, but also result in slightly reduced blood-myocardium contrast for balanced steady state free precession (bSSFP).

The relaxivities of exogenous agents have been measured at 0.55 T[16] and are reported in Table S1 in the Supplemental Material. Generally, gadolinium-based contrast agent relaxivity at 0.55 T is similar to 1.5 T, whereas large molecular weight contrast agents such as ferumoxytol have increased relaxivity at lower field strength. Current publications on low-field cardiac MRI have used standard dosing of gadolinium-based contrast agents and have speculated that lower doses of ferumoxytol may be feasible.[45]

Image Acquisition

Low field systems provide greater flexibility in pulse sequence design for cardiac MRI. Specific absorption rate (SAR) is a major constraint and is quadratic with field strength. This means that low-field MRI can utilize higher flip angles and more sophisticated RF pulse designs while staying within safety limits.[46] In a well-shimmed system, B0 inhomogeneity is dominated by susceptibility effects from the lungs and draining veins, and varies linearly with field strength.[47] The improved B0 homogeneity at low field enables the broad use of bSSFP, which suffers from banding artifacts at higher field strengths. Specifically, bSSFP acquisitions with longer TRs and lower receiver bandwidth are feasible without substantial banding and can be used to mitigate SNR loss.

Cardiac MRI generally benefits from motion-robust, efficient, data sampling. At conventional field strengths, spiral and echo-planar imaging have been employed, but their use is limited by off-resonance, which causes spatial blurring for spiral imaging, and warping for echo-planar imaging, and to a lesser extent, T2* signal decay during long readouts. At low field strengths, with more homogenous B0 and elongated

TABLE 3. Reported Cardiac T1, T2, and T2* Relaxation Times in Healthy Volunteers From 0.35 T,[44] 0.55 T,[16] 1.5 T,[16,44] and 3 T[44]

		0.35 T (msec)	0.55 T (msec)	1.5 T (msec)	3 T (msec)
Myocardium	T1	564	701	955	1200
	T2	59	58	49	40
	T2*	42	47	33	24
Arterial blood	T1	887	1122	1441	1808
	T2	386	263	254	120

T1 was measured with MOLLI[16] or Look-Locker[44] methods, T2 with T2-prepared bSSFP, and T2* with a multi-echo gradient echo sequence. Note that the relaxation times specified here are from the authors' study data and not meant to be interpreted as clinical reference values.

T2*, spiral and echo-planar readouts can be utilized to their full potential.[48] On modern 0.55 T systems, it is possible to use 6–8 msec spiral readouts with negligible blurring, a substantial improvement upon the 2–3 msec that has been used at 1.5 T. Spiral and echo-planar readouts can also be combined with bSSFP, with appropriate first moment nulling, to simultaneously capture high SNR efficiency, and high scan efficiency. High duty-cycle spiral acquisitions can also be combined with spectral-spatial excitations for fat suppression.[49] These RF pulses use spiral gradient waveforms for spatial and spectral encoding during excitation. The benefits of improved B0 and B1 homogeneity using a contemporary low field MRI system could therefore be applied for optimization of such RF pulses.

Image Reconstruction

A variety of modern denoising approaches can be employed at low field, including CS and artificial intelligence-based reconstruction. This is an area of active investigation across all field strengths, and denoising solutions are application specific. For example, ventricular function assessment should be done in a fashion that preserves fidelity of moving boundaries (eg, temporal finite difference constraint), and first-pass perfusion should be done in a fashion that preserves signal intensity time-course (eg, fit to a tracer-kinetic model).

Reduced artifacts at low field, eg, reduced blurring in spiral imaging, reduced banding in bSSFP and reduced susceptibility artifacts, can enable simpler reconstruction pipelines due to minimized correction steps. One exception is concomitant fields, which produce undesired spatially varying phase that is proportional to gradient amplitude and is inversely proportional to B0, making them more significant for low-field systems, particularly with high-performance gradients. The additional phase accumulation can be mitigated during image acquisition and/or corrected in reconstruction.[50,51]

It is expected that artificial intelligence-based image reconstruction and image enhancement will have a significant impact on image quality as low field MRI technology is further developed. For example, reconstruction with deep images priors can be used improve image quality for dynamic applications,[52] denoising and super-resolution have been demonstrated to enhance images,[53,54] and AUTOMAP has had significant success for image reconstruction at ultra-low field.[55]

Routine Cardiac MRI Sequences at Lower Field

A cardiac MRI exam typically consists of several pulse sequences depending on clinical indication, and this section will review the current literature and describe the ongoing efforts to translate the routine sequences used at 1.5 T to low-field MRI. Figures 2 and 3 provide example images of these routine cardiac MRI sequences from prototype and commercial 0.55 T systems, respectively. A comprehensive protocol for a commercial 0.55 T system with reduced gradient performance has also been described by Varghese et al.[20]

Cine Imaging

The measurement of chamber volume, systolic function, and ventricular mass using bSSFP cine imaging is a cornerstone of cardiac MRI exams and is clinically indicated in 92% of patients undergoing cardiac MRI.[56] Significant work has been done to develop and validate cine imaging for low field strengths. These studies suggest that, despite the lower SNR, low-field MRI can be accurately used for quantitative diagnostic evaluation of cardiac volumes and function and for assessment of regional wall motion abnormalities.

Bandettini et al studied a population of 65 participants, 44 clinically referred patients and 21 healthy volunteers, at 0.55 T (prototype system) and 1.5 T[19] (Fig. 2a; Video S1a in the Supplemental Material).[57] Quantitative comparisons of chamber volumes, ejection fraction and LV mass showed excellent correspondence between field strengths. A sector-wise comparison of regional wall motion abnormalities showed excellent agreement (kappa = 0.99). Varghese et al compared quantitative cine imaging, flow quantification and parametric mapping between 0.35 T, 1.5 T, and 3 T in healthy volunteers.[44] No significant difference in quantitative cine measurements of LV volume and function was reported. Zu et al also compared an AI-based analysis pipeline for endocardial and epicardial image contouring between 0.35 T, 1.5 T, and 3 T and found that the automated software performed well across field strengths.[58]

Other studies have focused on improving image acquisition strategies for cine imaging at lower field. Rashid et al explored high flip-angle bSSFP cine at 0.35 T and reported feasibility of flip angles up to 150°, with peak blood-myocardium CNR at 130°.[59] Restivo et al developed SNR-efficient spiral in-out and EPI bSSFP cine acquisitions for 0.55 T with high acquisition duty cycle (sampling time per TR).[48] They showed a 79% increase in myocardial SNR by moving from Cartesian bSSFP to spiral-in-out bSSFP imaging, with no change in breath-hold length or spatiotemporal resolution. Tian et al demonstrated a contrast-optimal simultaneous multi-slice (SMS) acquisition for breath-held cine.[46] They developed a spiral-out bSSFP sequence with SMS factors 2 or 3, and experimentally found peak blood-myocardium contrast at a flip angle of 160° for a single band and 120° for SMS acquisition.

CS has also been applied to improve cine image quality. Bandettini et al used an L1-SPiRIT image reconstruction for free-breathing cine and image quality was remarkably similar between 0.55 T and 1.5 T when using the same algorithm.[19] Simonetti et al used Sparsity adaptive COmpressive REcovery (SCoRe) for improved cine imaging at 0.35 T.[15] Vishnevskiy et al explored cine imaging at 0.75 T and retrospectively sparsely undersampled breath-held Cartesian cine data to evaluate high acceleration factors.[33] They were able to achieve

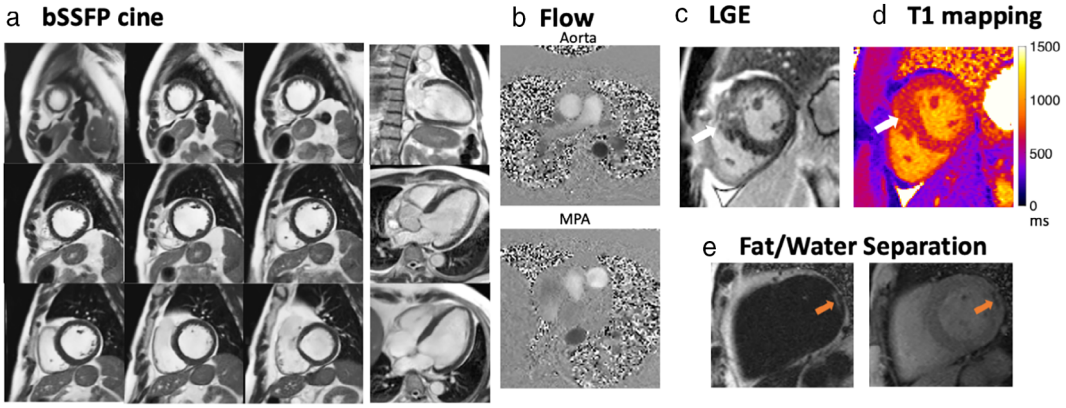

FIGURE 2: Example images from the prototype 0.55 T MRI system. (a) Free breathing bSSFP cine imaging of cardiac function using a compressed sensing image reconstruction (diastolic frame shown). This patient has a wall motion abnormality post myocardial infarction which can be seen in Video S1 in the Supplemental Material. (b) Flow quantification using phase-contrast MRI in the aorta and main pulmonary artery (MPA) in a patient with a ventricular septal defect. (c) Late gadolinium enhancement and (d) T1 mapping are shown in a patient with hypertrophic cardiomyopathy (white arrows). (e) Fat/water separation using the Dixon method in a patient with myocardial fat infiltration (orange arrows).

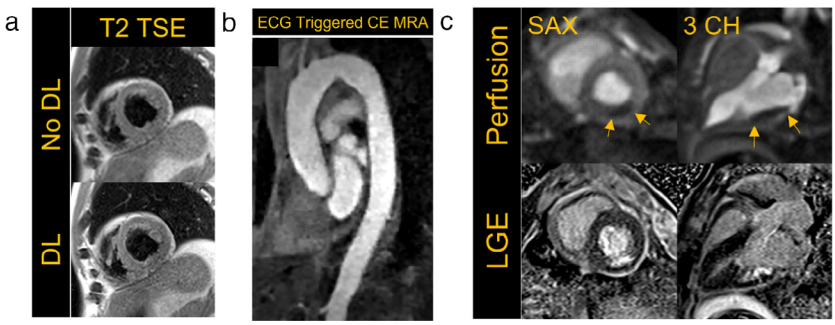

FIGURE 3: Example images from the commercial 0.55 T MRI system. (a) T2-weighted turbo spin echo (TSE) black blood imaging in a healthy volunteer with and without deep learning (DL) image enhancement. DL enhancements were vendor-provided reconstruction methods to densoise and increase image sharpness. (b) A compressed sensing-based ECG-triggered contrast-enhanced (CE) MR angiography (MRA) acquisition in a healthy volunteer. (c) Rest perfusion images and comparison late gadolinium enhancement (LGE) images illustrating a perfusion defect (arrows) in a swine model of myocardial infarction. [Adapted from Varghese et al[20]]

acceleration rates of 7 without image degradation. More recently, deep learning-based denoising has been applied to breath-held cine images with GRAPPA reconstruction. Specifically, a g-factor-savvy transformer convolution neural network model was used for GRAPPA reconstruction with acceleration rate of 3 on a commercial 0.55 T system, with more than double the original SNR.[54,60] Future work on deep learning-based denoising and imaging reconstruction is expected to further improve image quality.

Real-time cine, which is neither ECG gated nor breath-held, has also been developed for low field strengths. Hamilton et al used a deep image prior reconstruction based on two U-nets to generate spatial and temporal basis functions for real-time cine images from highly undersampled spiral acquisitions on the commercial 0.55 T system.[52] Their method used a spatial resolution of 2.2 mm and they compared five acceleration rates from $R = 4$ (76 msec temporal resolution) to $R = 24$ (13 msec temporal resolution). A spiral in-out bSSFP acquisition has been paired with a low rank + sparse image reconstruction on a prototype 0.55 T for real-time cine with a spatial resolution of 1.7 mm and temporal resolution of 36 msec.[61] Yagiz et al developed real-time cine with SMS factor 3 and a flip angle of 100°, paired with a constrained image reconstruction.[62] A realistic simulation framework, based on the XCAT phantom, has also been proposed and used to simulate real-time volumetric (3D) cine at 0.55 T with a stack-of-spirals trajectory.[63]

Finally, Piccini et al performed a proof-of-concept free-breathing motion-resolved 3D imaging study at 0.55 T.[64] This acquisition used a 3D radial trajectory with superior–inferior readouts for extraction of cardiac and respiratory self-navigation signals that were used to sort data into 20 cardiac and 4 respiratory bins. Isotropic spatial resolutions of 1.1 to 2.0 mm^3 were visually compared and 3D images were re-sliced into cardiac views.

Flow Quantification

Phase-contrast flow imaging is commonly used clinically for quantitative metrics such as cardiac output and for characterizing valvular heart disease. Flow imaging uses a T1-weighted

spoiled gradient-echo sequence and inflow enhancement during systole, and benefits from the shorter T1 at lower field. The effect of concomitant fields can result in additional phase distributions across the imaging plane.[65] However, as these fields are predictable, and can be corrected using several approaches, this should not lead to quantification errors.[3]

Comparison studies have shown accurate measurements of cardiac output for both aortic and pulmonary artery measurements at low field. Varghese et al compared breath-held aortic flow measurements and found no statistically significant differences in cardiac output measurements at 0.35 T, 1.5 T, and 3 T in six healthy volunteers.[44] The 0.35 T:3 T relative SNR was higher than would be predicted from polarization alone. Shanbhag et al studied pulmonary and systemic flow in 10 healthy subjects and 8 patients referred for valvular or shunt evaluations at 0.55 T (Fig. 2b; Video S1b in the Supplemental Material).[66] A high correlation between flow measured at 0.55 T and 1.5 T was measured across all subjects, and Bland–Altman analysis showed reasonable agreement in cardiac output, and the ratio of pulmonary-to-systemic flow.

Research studies have explored using a bSSFP acquisition paired with flow-encoding, exploiting low-field's improved field homogeneity for relatively long-TR steady-state imaging. Using bSSFP eliminates the inflow-driven contrast of GRE and therefore provides more consistent SNR across the cardiac cycle. However, this technique can present difficulties in quantification due to spatial phase errors induced by bSSFP acquisitions.[67] Ramasawmy et al demonstrated a bSSFP-flow acquisition using a spiral-readout to maximize the SNR at 0.55 T in 11 volunteers[68] and Peper et al compared a Cartesian bSSFP-flow acquisition to gradient-echo at 0.75 T in 6 volunteers.[69]

Late Gadolinium Enhancement

LGE imaging is the standard for noninvasive detection of scar tissue and the assessment of myocardial viability,[70] and is an important component of most clinical cardiac MRI exams. LGE images are acquired at end-diastole, and can either involve segmented breath-held acquisitions, or fast "snapshot" imaging for free-breathing approaches. Snapshot imaging speed is limited at low field due to reduced SNR, reduced gradient performance on some commercial systems, and low acceleration factors from limited coil arrays.

Bandettini et al compared breath-held, phase-sensitive inversion recovery LGE image quality and diagnostic assessment between a high-performance 0.55 T and 1.5 T in 16 patients with myocardial infarction (MI).[18] A bSSFP acquisition was used at low-field to improve SNR (Fig. 2c). A strong correlation was measured between field strengths for absolute LGE mass and percentage MI, and no significant bias was found between measurements of MI mass from Bland–Altman analysis. A recent case study demonstrated LGE imaging on a commercial, lower gradient-performance 0.55 T scanner in a case of nonischemic fibrosis.[71] In addition, Ding et al presented a CS based technique that incorporates motion fields along with the reconstruction, leading to increased sharpness in free-breathing LGE acquisitions in 12 volunteers on a commercial 0.55 T system.[72]

Parametric Mapping and ECV Fraction

MRI parametric mapping of T1, T2, and T2* relaxation times and ECV fraction of the myocardium facilitates characterization and monitoring of diseases such as fibrosis, amyloidosis and iron overload.[73] Parametric mapping is typically acquired during the end-diastolic window with a "snapshot" imaging technique. Though the relaxation rates will vary, with T1 being shorter, and T2 and T2* times being longer at lower field strength, the magnetization preparation schemes used for parametric mapping are not significantly altered for imaging across different field strengths.

Campbell-Washburn et al measured tissue T1, T2, and T2* relaxation times including myocardium and arterial blood in 39 subjects using breath-held imaging at 0.55 T,[16] and Varghese et al reported T1, T2, and T2* at 0.35 T, compared to 1.5 T and 3 T, in six healthy volunteers.[44] Mancini et al measured native and post gadolinium contrast T1, and ECV in 27 subjects, including 13 patients with MI, across 0.55 T and 1.5 T (Fig. 2d).[74] Native and post-contrast T1 relaxation times were shorter at 0.55 T, as expected, with the relative gadolinium induced T1 shortening being approximately 20% greater at 0.55 T. Both T1 relaxation times and ECV had a fair correlation between 0.55 T and 1.5 T across the regions of interest including remote myocardium and infarcted tissue. Crabb et al assessed a prototype 3D whole-heart spiral sequence for joint T1/T1ρ mapping and water-fat imaging on the commercial 0.55 T system and demonstrated promising in vivo results.[75]

Varghese et al demonstrated myocardial T2 mapping in a porcine model of ischemia–reperfusion induced MI in five animals at 0.55 T.[76] The authors demonstrated the breath-held acquisition, and measured significant elevation in T2 within the infarct regions compared to remote myocardium.

T2* and R2* have gained acceptance for noninvasive assessment of iron overload in the liver and in the heart.[77,78] Due to the improved field homogeneity of contemporary low-field MRI systems, T2* relaxation times are expected to be longer, and R2* values smaller, which could potentially offer improved sensitivity in patients with severe iron overload that is difficult to accurately quantify at 1.5 T or 3 T. Campbell-Washburn et al performed a comparison study of hepatic R2* mapping between 0.55 T and 1.5 T in patients with iron overload, and showed significantly smaller R2* at 0.55 T as expected, reasonable measurement precision, and accurate assessment of liver iron content.[79] A predictive model was used to predict R2* across field strengths, which could be extended to other field strengths as well.[80]

Fat-Water Separation

Myocardial fat infiltration, and epicardial adipose tissue has been linked to an increased risk of cardiovascular disease, including sudden cardiac death and coronary artery disease.[81] Separating fat and water peaks is more difficult at lower fields due to the converging chemical frequencies. In addition, the shorter T1 relaxation times at low field will mean that fat, typically the shortest T1 species found in the body, will have increased signal amplitude and will require a narrow signal null period for inversion-recovery-based methods for fat-suppression, though these have been demonstrated at 0.55 T for abdominal imaging.[82] Dixon-based methods require longer time intervals between echoes with smaller chemical shift effects, which can limit the sampling frequency for cardiac imaging, but have been successfully demonstrated at 0.55 T for both cardiac and abdominal applications (Fig. 2e).

Non-Cartesian trajectories that can resolve the spectra have been explored, such as by Franson et al, who demonstrated a rosette trajectory,[83] and Tian et al, who proposed a novel multi-echo spiral acquisition.[84] Both these trajectories demonstrated good fat-water separation using relatively long TRs (10–12 msec) possible with bSSFP at 0.55 T.

Cardiac and Vascular Morphology

Cardiac morphology is assessed using black-blood T2-weighted imaging, especially for the evaluation of tumors and masses. Varghese et al optimized T2-weighted turbo spin echo (TSE) sequences for the commercial 0.55 T system (Fig. 3a).[20] TSE performed well with little modification since it is a high SNR technique and is not particularly demanding on system performance.

Three-dimensional thoracic vascular morphology is typically imaged using contrast-enhanced or non-contrast MR angiography (MRA). Varghese et al demonstrate non-contrast MRA using a ECG-triggered 3D bSSFP with T2 magnetization preparation and fat suppression, and contrast-enhanced MRA (Fig. 3b) with a CS-accelerated breath-held 3D spoiled gradient echo sequence at 0.55 T.[20] Castillo-Passi et al evaluated a proof-of-concept non-contrast motion-corrected 3D whole-heart MRA sequence and achieved reasonable image quality in 6 minutes at 0.55 T.[85]

Perfusion

First-pass perfusion imaging of the myocardium during rest and pharmacological stress has excellent sensitivity for detecting myocardial ischemia and there is growing evidence supporting the use of this technique for diagnostic cardiac MRI. Contrast-enhanced perfusion relies on fast, saturation-recovery, gradient-echo, and bSSFP snapshot acquisitions, ideally with a temporal footprint <80 msec. Rapid imaging is especially crucial for performing perfusion imaging during pharmacological stress at higher heart rates. For quantitative imaging, these snapshot acquisitions can be additionally paired with a low-resolution acquisition which measures the arterial-input function.[86] The translation of this technique to low field requires care as this technique is already in the low SNR regime at 1.5 T. Simulations regarding perfusion have demonstrated viability of this technique at 0.55 T.[63] Varghese et al demonstrated the use of a CS reconstruction with acceleration rate 5 to achieve snapshot gradient echo images with a <110 msec temporal footprint for perfusion imaging at rest at 0.55 T (Fig. 3c).[20] The authors illustrated the successful depiction of a resting perfusion defect in a patient with known MI.

Strain-Encoded Imaging

Left and right ventricular strain characterizes myocardial contractility, and may provide early detection of cardiac dysfunction, prior to overt functional or structural changes.[87] Strain-encoded MRI (SENC) is a reproducible method of directly measuring strain,[88] but as the encoding method results in an inherently low SNR image, its feasibility is questionable at low field. A prototype sequence has been validated with the commercial 0.55 T system using a dynamic gel deformation phantom, and feasibility has been successfully assessed in a small cohort of healthy volunteers and in a porcine ischemia–reperfusion infarct model (Fig. 4).[90]

Advanced Cardiac MRI Applications

There are several new opportunities to leverage the unique properties of low field strength to expand the application of cardiac MRI beyond the current clinical routine. This

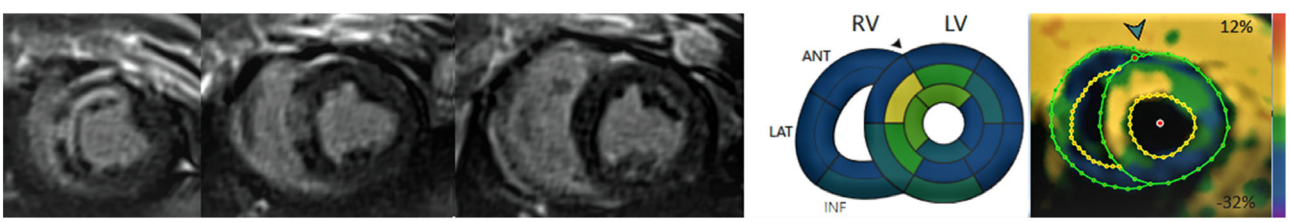

FIGURE 4: Strain images from a commercial 0.55 T MRI system. The left panel shows Late Gadolinium Enhanced images in a porcine myocardial infarction model, showing apical, antero-septal infarct caused by 90-minute occlusion followed by reperfusion of the left anterior descending coronary artery. The AHA 16-segment bulls-eye plot in the middle shows longitudinal strain deficit (in yellow and green) in the segments corresponding to the infarct location. The corresponding apical short-axis SENC image in the right panel shows the longitudinal strain deficit in the anterior septal region. [Reproduced from Liu et al.[89]]

section will describe example advanced applications of low-field cardiac MRI.

MRI-Guided Invasive Procedures

MRI-guided cardiac catheterization procedures use real-time MRI to guide catheter-based devices in the heart. MRI-guided hemodynamic right heart catheterization (chamber pressure measurement) has been demonstrated in hundreds of adult and pediatric patients,[91–96] and more recently, the first patient demonstrations of MRI-guided electrophysiology and RF ablation have been performed.[97–99] There have also been many pre-clinical studies exploring the advantages of MRI-guidance for other procedures such as endomyocardial biopsy, stenting, ventricular tachycardia (VT) ablation, extra-anatomic bypass, etc.[100–103] Most off-the-shelf catheterization devices contain long metallic components and are susceptible to RF-induced heating, and there are few custom-built devices approved for human use. Patient MRI-guided catheterization has been accomplished mainly with polymer catheters. The paucity of devices that are MR-safe and mechanically adequate has hampered the clinical translation of many of these procedures.

Lower fields offer reduced RF-induced heating of metallic devices, and therefore may enable new procedures using off-the-shelf devices or simplify the design of custom-built devices. Most work on low-field MRI-guided catheterization procedures has been performed on a prototype 0.55 T system with high performance gradients. Heating is quadratically related to field strength, meaning that 0.55 T offers 7.5-fold less device heating than 1.5 T, and 30-fold less device heating than 3 T.[16,104]

Campbell-Washburn et al demonstrated MRI-guided right heart catheterization at 0.55 T in seven patients.[16] Importantly, they used off-the-shelf metallic guidewires (fully insulated nitinol guidewires) without modification to the devices or to the real-time bSSFP imaging parameters (flip angle = 45°, TR = 4 msec). They measured <1°C of heating during 2 minutes of real-time imaging in 9 of 16 test nitinol guidewires and stainless-steel braided catheters. Recently, Özen et al systematically evaluated device safety for several off-the-shelf devices (guidewires, catheters, needles, and microwave applicator) and found negligible heating at 0.55 T.[104]

Kolandaivelu et al assessed the visibility of chemoablation lesion and RF-ablation lesions at 0.55 T in a porcine model as a precursor to MRI-guided ablation at low field (Fig. 5).[105] The ability to visualize and assess ablation lesions is a key advantage of MRI-guidance over X-Ray guidance of these procedures.[106] Seemann et al performed invasive pressure-volume loop measurements at 0.55 T during dynamic inferior vena cava occlusion to alter preload conditions.[107] The technique combines simultaneous real-time imaging to measure cardiac volumes and invasive measurement of pressure to generate pressure-volume loops. This work was performed in three pig models: naïve, ischemic cardiomyopathy, aortic banding to increase afterload, and illustrated lower cardiac contractility and higher compliance in cardiomyopathy.

Visualization of metallic devices using susceptibility artifacts alone can be challenging at 0.55 T. The artifact profile of low-susceptibility materials (eg, nitinol, stainless steel 316) are reduced at 0.55 T, whereas those of high-susceptibility materials (eg, stainless steel 304) are consistent across field strengths because they are already saturated below 0.55 T.[108] Pilot studies have investigated computer vision methods to improve the detection of nitinol devices at 0.55 T.[109,110] Custom devices with built-in receiver electronics designed for "active" visualization are attractive to improve sensitivity and specificity of device visualization. Design constraints related to RF-induced heating are eased at 0.55 T, allowing for increased flexibility in device configuration. A safe-by-design active guidewire with continuous shaft-to-tip profile that is mechanically comparable to off-the-shelf devices has been demonstrated for 0.55 T.[111] Additionally, a new technique of thin-film printed circuitry which can fabricate RF antenna components direction onto metallic surfaces with conductive ink has been demonstrated for needle devices at 0.55 T.[112]

Most recently, interventional studies on a commercial 0.55 T system has demonstrated promising real-time imaging results despite the reduced gradient performance. Armstrong et al demonstrated cardiac catheterization, angioplasty, and stenting on the commercial 0.55 T (Fig. 6; Video S2 in the Supplemental Material).[113] Mooiweer et al demonstrated the feasibility of real-time proton resonance frequency shift-based thermometry. MRI thermometry is a common method to assess thermal ablation treatments in real-time, and therefore is an essential tool for application of low-field MRI for cardiac ablation procedures.[114]

MRI-Guided Radiotherapy

Hybrid MRI-guided radiotherapy systems (MR-linacs) have also been applied for cardiac interventional procedures. Specifically, a 0.35 T ViewRay MRI-linac system was used for MRI-guided stereotactic ablative radiotherapy of ventricular tachycardia. The first-in-human procedure was performed in a patient with dilated cardiomyopathy and recurrent sustained ventricular tachycardia with a cardiac implantable cardioverter-defibrillator (Fig. 7).[115] Motion tracking was performed with the upper liver and procedural planning used invasive electroanatomical mapping and prior cardiac MRI. The patient received a single fraction of 25 Gy, with cine-tracking time of 46 minutes and beam-on time of 24 minutes. Since the initial case report, additional studies have explored cardiorespiratory motion management for MRI-guided radioablation procedures a 1.5 T that may also have applicability at lower field.[116]

Combined Cardiopulmonary Assessment

Contemporary low-field MRI systems using superconducting magnets can provide improved B0 field homogeneity

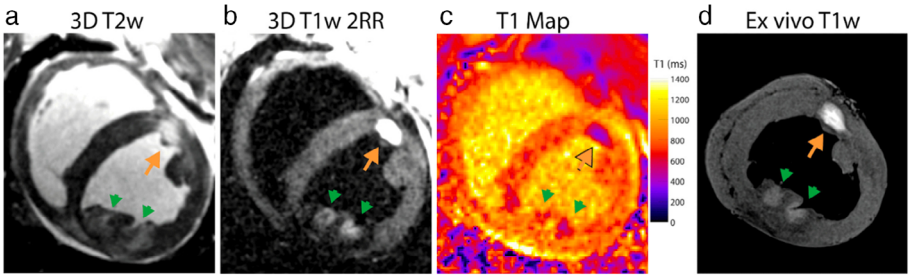

FIGURE 5: Assessment of RF ablation lesions (green arrows) and chemoablation lesions (orange arrows) on a prototype 0.55 T MRI system in a swine model. In vivo imaging included (a) 3D T2-weighted imaging, (b) 3D T1-weighted imaging, (c) T1 mapping, and ex vivo imaging used (d) 3D T1-weighted imaging to confirm the location of the lesion in fixed tissue. [Reproduced from Kolandaivelu et al.[105]]

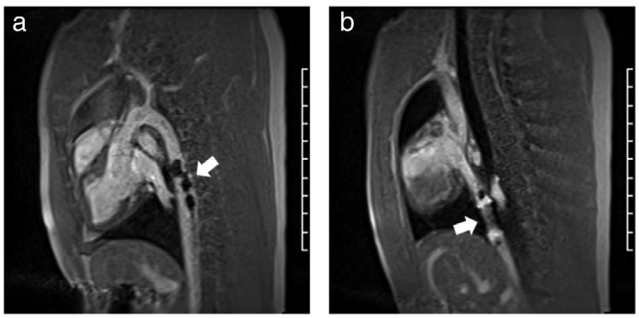

FIGURE 6: MRI-guided procedure using commercial 0.55 T MRI system in a swine model. (a) MRI-conditional polymer guidewire with susceptibility markers (arrow) (EmeryGlide, Nano4Imaging, Aachen, Germany) used for MRI-guided left heart catheterization, and (b) placement of a stent in the inferior vena cava (arrow) (Z-Med Balloon, NuMED for Children, Orlando, FL). Real-time imaging was achieved with spoiled gradient echo (~2 frames/s, 1.8 mm × 2 mm × 9.5 mm) following administration of 2 mg/kg ferumoxytol.

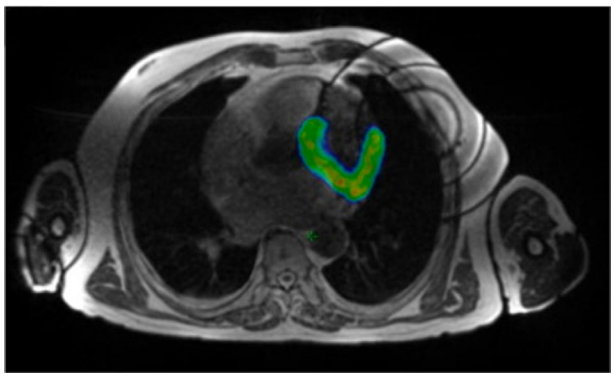

FIGURE 7: Example images from the first-in-human MRI-guided radioablation at 0.35 T with estimated delivered radiation dose overlaid. [Adapted from Mayinger et al.[115]]

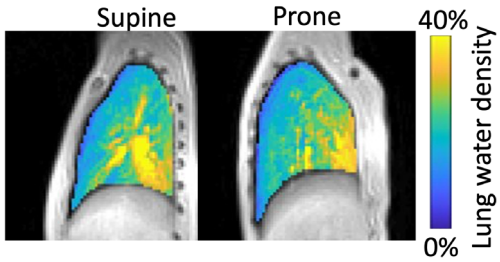

FIGURE 8: Quantitative lung water density measurement with the patient supine and prone to illustrate the gravitational dependence of lung water distribution. The evaluation of cardiogenic pulmonary edema is valuable during the MRI assessment of heart failure.

compared to 1.5 T or 3 T, which translates to reduced susceptibility gradients in anatomy with air-tissue interfaces, such as the lung, thereby providing an attractive environment for pulmonary imaging. Imaging the heart and lung in the same setting can be valuable for assessment of cardiopulmonary interactions, especially when paired with exercise and hemodynamic catheterization as appropriate. Work has been done to demonstrate structural and functional lung imaging at 0.55 T and 0.35 T,[117–120] including the assessment of oxygen-enhanced MRI[121] and ventilation/perfusion (V/Q) imaging.[122–124]

For the assessment of patients with heart failure, Seemann et al optimized and validated a stack-of-spiral ultrashort echo time (UTE) sequence for the quantification of lung water density with an automated inline image processing pipeline at 0.55 T (Fig. 8).[125] Cardiogenic pulmonary edema is the pressure-driven accumulation of fluid in the pulmonary interstitium which causes breathlessness and is a key feature of heart failure. Moreover, this technique was extended to measure dynamic changes in lung water during exercise stress, since exercise intolerance is an early symptom of cardiogenic pulmonary edema.[126] Measurements of lung water can be combined with the routine assessment of heart failure by cardiac MRI.

Imaging Patients With Implants

The reduced susceptibility artifacts of contemporary low-field MRI systems can also be leveraged for reduced artifacts in the growing population of patients with implants and devices. Bandettini et al performed a pilot study comparing image artifacts caused by implants between 1.5 T and 0.55 T (Fig. 9).[127] As expected, they observed smaller and less disruptive image artifacts at 0.55 T for most devices, however, the amount of artifact reduction depends on the implant material. Keskin et al demonstrated the feasibility of gradient-echo-based sequences, including bSSFP, for near-metal imaging at 0.55 T.[128] Van Speybroeck

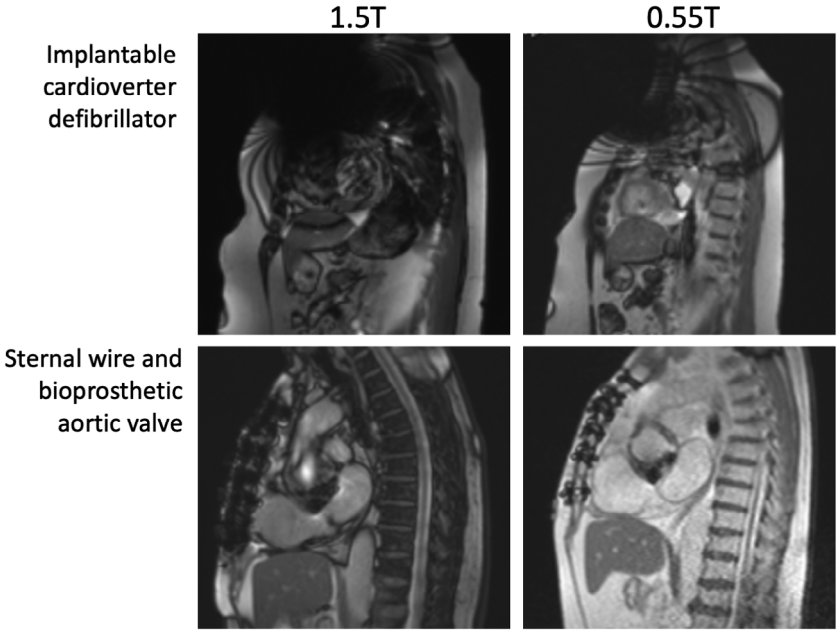

FIGURE 9: Comparison of artifacts caused by metallic implants at 1.5 T and 0.55 T. [Adapted from Bandettini et al[127]]

et al demonstrated susceptibility artifacts for a 50 mT permanent magnet system in phantoms.[129] To date, few devices are labeled for low-field MRI. While the general assumption is that low field is safer than higher field strengths, safety has a complex dependence on device length/RF wavelength and system geometry and thus safety testing is still required.[130,131]

Imaging Obese Patients

Contemporary cardiovascular medicine heavily relies on noninvasive imaging by echocardiography, CT, SPECT, and MRI. Unfortunately, severely obese patients are difficult and sometimes impossible to assess by any cardiovascular imaging modality for a variety of reasons.[132,133] In a recent study in patients with a mean BMI = 43 undergoing SPECT myocardial perfusion imaging, 32.6% of the studies were non-diagnostic.[134] While CT scanners with 80 cm and larger bore diameter are available, CT of severely obese patients can suffer from truncation and cropping artifacts.[135] CT radiation dose may be increased by factors of 3 or more in morbidly obese patients,[136] and five times higher for fluoroscopy.[137] Furthermore, it may not be practical or safe to administer contrast agents or radioisotope dose based on body weight in the largest patients.[138,139] While echocardiography has no table or bore restrictions, it may be the modality most limited by severe obesity.[133,138,139] Increased body thickness decreases beam penetration, and thick layers of fat that attenuate the signal at a rate of 0.63 dB/cm further reduce signal-to-noise.[133,139]

In MRI, larger patients who fit tightly into the scanner may not be properly insulated from the magnet bore to prevent burns.[140,141] Severely obese patients may be unable to lie supine for extended periods, may have significant trouble with extended or repeated breath-holding, and ECG signal may be attenuated.[142] Thus, the potential benefits of MRI with its versatile diagnostic and prognostic capabilities[143,144] are unavailable to a large segment of the population at high risk for CVD.

The greater flexibility in magnet design at low field makes wider, more open bore configurations possible, eliminating the primary barrier to MRI for these patients. Low-field MRI may thus become the cardiac imaging modality of choice in these patients who often have no other options.[145–147] Varghese et al[20] demonstrated the potential clinical utility of cardiac imaging on an 80 cm bore commercial 0.55 T system in two patients unable to be scanned on a standard 70 cm bore system due to their large body habitus; image results are shown in Fig. 10 and Video S3 in the Supplemental Material. Patient A, having a weight of 350 lbs and BMI = 48 kg/m^2, was unable to be scanned in a 70 cm bore due to physical discomfort and anxiety. As shown in the figure, prior echocardiography images were of poor quality, even with the use of contrast. Conversely, the bSSFP cine, breath-held segmented LGE, and contrast-enhanced aortic MRA demonstrated good quality and diagnosis of cardiomyopathy and dilated aorta. In the second patient shown (Patient B), weighing 410 lbs and having BMI > 57 kg/m^2, cine, flow, and LGE images were successfully acquired on the 80 cm bore 0.55 T system and revealed normal biventricular systolic function but also identified nonischemic fibrosis. Both patients reported being comfortable throughout the exam and demonstrate how valuable diagnostic information could be provided by low-field MRI when other cardiac imaging was not an option.

Fetal Cardiac Imaging

Fetal imaging at low field appears promising for several reasons. The potential for a wider bore is beneficial for maternal

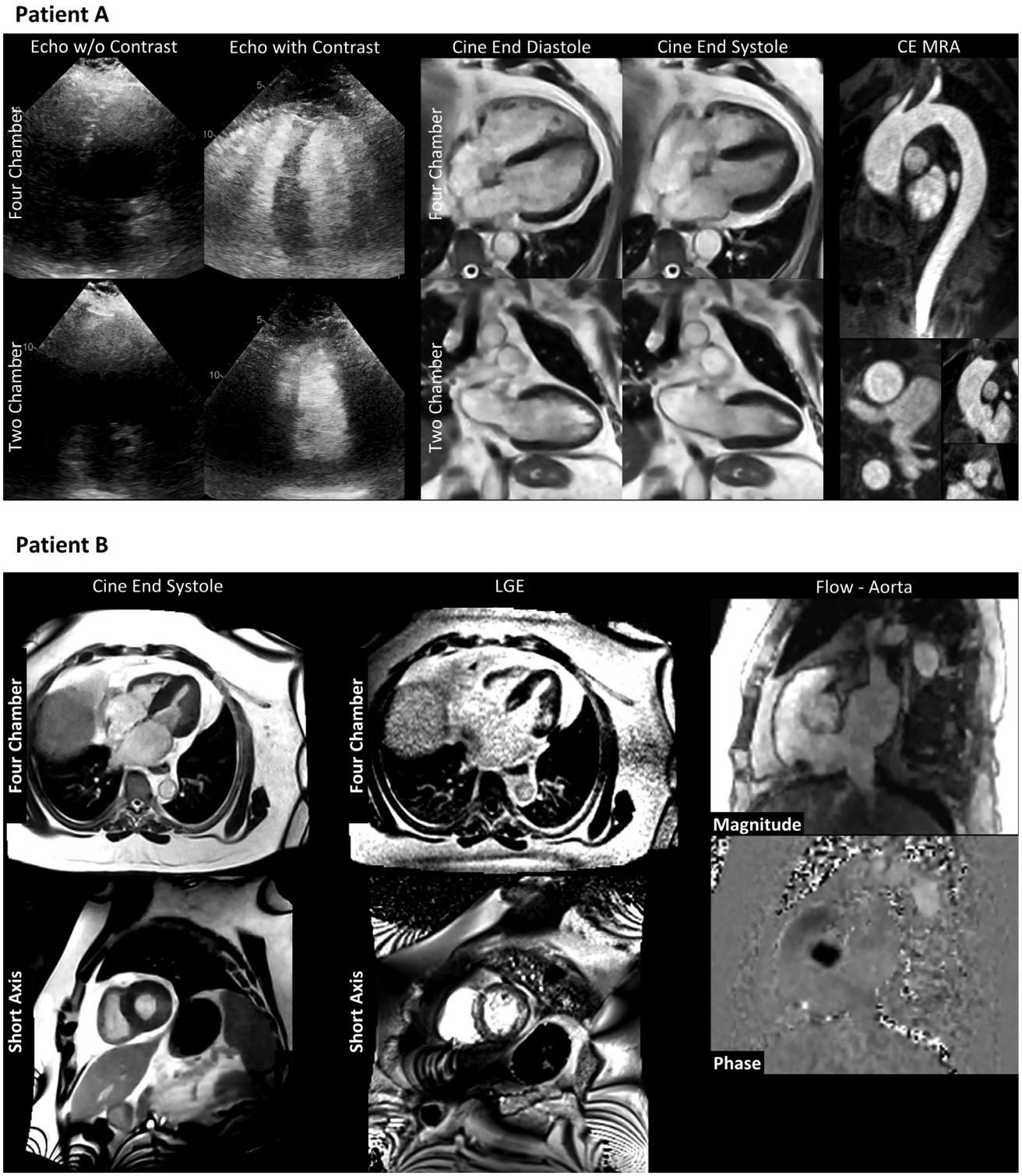

FIGURE 10: Example images from a commercial 80 cm bore, 0.55 T system in two obese patients unable to undergo cardiac MRI assessment on 70 cm bore systems due to body habitus. Patient A (Male, 61 y.o., 350 lb, BMI 48 kg/m^2, body surface area 2.6 m^2)—Breath-held segmented cine images in four and two-chamber views are shown along with the patient's echocardiographic images, acquired without and with ultrasound contrast. Multiplanar reformatted images of the thoracic aorta acquired with a non-triggered contrast-enhanced MR angiogram depicts a dilated aorta. Patient B (Male, 6.5.y.o., 410 lbs, BMI > 57 kg/m^2, body surface area 2.86 m^2)—Breath-held segmented cine (four chamber and short axis view), free-breathing motion-corrected (four chamber) and breath-held segmented (short axis) LGE demonstrating fibrosis, and magnitude and phase images of the aortic root are shown. [Adapted from Varghese et al.[20] and Simonetti et al.[148]]

comfort. The reduced acoustic noise and reduced SAR is beneficial from the fetal motion and safety perspective, and the improved real-time MRI is beneficial since most imaging is performed without fetal cardiac gating. Hutter et al reported on the first 150 fetal MRI scans at 0.55 T for noncardiac imaging.[149] Recently, it has been shown that fetal cardiac function and anatomy can be captured in real-time at 0.55T without requiring retrospective gating that is typical at 1.5 T and 3 T.[150] Furthermore, metric optimized retrospective gating can successfully recover SNR at 0.55T when targeting finer spatial resolutions, or in low SNR scenarios (eg, underlying maternal obesity).[151] Finally, 4D reconstructions can be generated from these data.[152] At this point, feasibility has been demonstrated, and larger numbers of cases are needed to determine clinical potential.

Future Advanced Cardiac MRI Applications

Three-dimensional coronary imaging with MRI is of great interest to evaluate coronary artery disease, and to identify coronary anomalies in congenital heart disease. Coronary imaging relies on sub-millimeter spatial resolution, which presents a challenge for low field MRI. Several recent publications have demonstrated whole-heart free-breathing imaging with reasonable acquisition and reconstruction times.[153] The capability of low field MRI to identify coronary arteries and characterize coronary anomalies remains of-interest, and advanced data sampling and image reconstruction techniques will likely be required to address this demanding application.

Multi-dimensional multi-contrast techniques, such as MRI fingerprinting[154] and MR multitasking,[155] are attractive for low field cardiac MRI. These techniques may allow "push button" imaging that generates several parameters of interest from a single acquisition, thereby making accessible low field MRI easier to use. MR fingerprinting typically relies on spiral imaging which performs well at low field, and dictionary matching which tends to be less sensitive to low-SNR regimes. MR fingerprinting has been demonstrated for noncardiac applications at field strengths from 6.5 mT to 0.55 T.[156–159] While there are no publications on cardiac MR fingerprinting or multi-tasking to-date, there remains significant interest in this area.

Discussion

Low-field MRI systems offer significant promise to enable routine cardiac MRI in underserved geographical regions and patient groups with limited access to cardiac MRI previously, as well as to reduce siting requirements for point-of-care imaging. Studies to-date confirm that low-field MRI offers high measurement concordance and consistent interpretation with clinical 1.5 T imaging. Moreover, low-field MRI may enable specific new clinical imaging opportunities, beyond what is possible at 1.5 T, due to certain favorable imaging properties.

Increased accessibility by virtue of lower system cost is one of the key advantages of low-field MRI, however the exact cost can be hard to predict. The cost to manufacture a lower field superconducting magnet for whole body MRI is inherently lower since less material is required. Siting costs such as floor reinforcements are also inherently lower because these systems are lighter weight. Low-field systems can be equipped with cooling technology that uses low levels of helium and thus avoid a quench pipe.[31] However, other costs such as gradient hardware, system electronics, room shielding, computers, and operating costs are expected to be similar for current whole-body system designs. If other compromises are made, costs could be further reduced, but may sacrifice performance for cardiac imaging applications. Overall, low-field MRI systems designed for cardiac imaging will be of lower cost than the current clinical standard, but the exact cost will depend on system specifications and design.

This article has focused on superconducting cylindrical whole-body MRI systems used for cardiac MRI, however operating a lower field enables more flexibility in magnet design. Outside the heart, low-field and ultra-low field systems have been designed with varied bore geometries, including vertical bores, single-sided systems, and planar systems. Unfortunately, these non-standard geometry systems often lack the field homogeneity and gradient performance needed for cardiac applications. Hypothetically, one could imagine low-field MRI designed with a short and wide bore for patients with claustrophobia undergoing cardiac MRI, or a vertical bore system for upright and/or exercise imaging.

Low-field whole-body MRI systems can also be used for other applications within the radiology setting including routine body imaging, musculoskeletal imaging, and neuroimaging, and specialized tasks such as pulmonary imaging, and imaging near metal implants. The availability of low-field MRI systems may alter how systems are selected and deployed within radiology departments.[160] Alternatively, large cardiology centers may opt to install low-field MRI systems directly in cardiology departments.

Increased system accessibility could increase the demand for trained cardiac MRI technologists or radiographers to operate the scanners. In parallel, accessibility could drive improvements in automated slice planning and quality assurance. Advanced technology that is under development, such as push-button isotropic multi-contrast 3D scanning, could also simplify cardiac imaging in the hands of non-experts.

Low SNR due to the reduced equilibrium polarization proportional to B0, is an obvious disadvantage of low field. As discussed here, low SNR can be partially compensated by switching from GRE to bSSFP and moving from Cartesian to spiral or echo-planar readouts and by incorporating advanced image reconstruction techniques. However, these solutions

may not be applicable or adequate for some cardiac imaging techniques, especially SNR-starved ones such as cardiac diffusion imaging, and cardiac spectroscopy. Low field is additionally problematic for advanced applications that benefit from spectral shifts, short T2* relaxation times and/or long T1 relaxation times at conventional field strengths. This includes proton spectroscopy that can assess myocardial triglycerides using chemical shift, although this has been demonstrated at 0.75 T.[30] This also includes arterial spin labeling (ASL),[161] and blood-oxygen level dependent (BOLD) imaging,[162] both nascent approaches for detecting ischemia without contrast agents at conventional field strengths.

Another challenge of low-field MRI is concomitant field effects. For gradient-echo imaging, these effects can be mitigated with frequency-segmented deblurring or an expanded signal model reconstruction.[50,163] Effects have been mitigated for rapid acquisition of recalled echoes (RARE, also known as fast spin echo or TSE), using compensatory gradient pulses.[164,165] This issue is not fully resolved for bSSFP and mitigation approaches are necessary, such as decreasing gradient amplitudes.[51]

Low-field MRI offers significant promise for cardiac MRI, both to reduce cost and enable new applications. Basic cardiac sequences are ready to be used for clinical evaluation at low field, while more advanced cardiac imaging techniques need further optimization and development. Further clinical studies establishing reference parametric values and assessing the diagnostic accuracy of low-field MRI across a range of techniques and patient populations are warranted. Additionally, techniques designed for challenging patients, like those with arrhythmia or those unable to hold their breath, require evaluation and validation before low-field cardiac MRI can be broadly adopted. There are still significant opportunities to improve image acquisition and reconstruction techniques to leverage the specific physical properties of low-field MRI, and there are opportunities to translate computational methods developed for higher field strengths to be applied at lower field strengths. Substantial advancements in both imaging methods and clinical applications are anticipated for low-field cardiac MRI over the next several years.

Acknowledgments

This publication was supported, in part, by the National Heart, Lung, and Blood Institute (NHLBI) of the National Institutes of Health (R01HL161618) and the NHLBI Division of Intramural Research (Z01-HL006257, Z01-HL006213).

Conflict of Interest

Adrienne E. Campbell-Washburn and Rajiv Ramasawmy are investigators on a US Government Cooperative Research and Development Agreement (CRADA) with Siemens Healthcare. Krishna S. Nayak receives funding from Siemens Healthcare. Orlando P. Simonetti receives funding from Siemens Healthcare, Nano4Imaging, and NuMED. Siemens participated in the modification of the prototype MRI systems from 1.5 T to 0.55 T.

References

1. Leiner T, Bogaert J, Friedrich MG, et al. SCMR Position Paper (2020) on clinical indications for cardiovascular magnetic resonance. J Cardiovasc Magn Reson 2020;22(1):76.
2. Couto M, Souto M, Martinez A, et al. Accuracy of right ventricular volume and function assessed with cardiovascular magnetic resonance: Comparison with echocardiographic parameters. Clin Imaging 2020; 59(1):61-67.
3. Nayak KS, Nielsen JF, Bernstein MA, et al. Cardiovascular magnetic resonance phase contrast imaging. J Cardiovasc Magn Reson 2015; 17:71.
4. Simonetti OP, Kim RJ, Fieno DS, et al. An improved MR imaging technique for the visualization of myocardial infarction. Radiology 2001; 218(1):215-223.
5. Aquaro GD, Ghebru Habtemicael Y, Camastra G, et al. Prognostic value of repeating cardiac magnetic resonance in patients with acute myocarditis. J Am Coll Cardiol 2019;74(20):2439-2448.
6. Spieker M, Haberkorn S, Gastl M, et al. Abnormal T2 mapping cardiovascular magnetic resonance correlates with adverse clinical outcome in patients with suspected acute myocarditis. J Cardiovasc Magn Reson 2017;19(1):38.
7. Yang F, Wang J, Li W, et al. The prognostic value of late gadolinium enhancement in myocarditis and clinically suspected myocarditis: Systematic review and meta-analysis. Eur Radiol 2020;30(5):2616-2626.
8. Greenwood JP, Maredia N, Younger JF, et al. Cardiovascular magnetic resonance and single-photon emission computed tomography for diagnosis of coronary heart disease (CE-MARC): A prospective trial. Lancet 2012;379(9814):453-460.
9. Kwong RY, Ge Y, Steel K, et al. Cardiac magnetic resonance stress perfusion imaging for evaluation of patients with chest pain. J Am Coll Cardiol 2019;74(14):1741-1755.
10. Esposito A, Gallone G, Palmisano A, Marchitelli L, Catapano F, Francone M. The current landscape of imaging recommendations in cardiovascular clinical guidelines: Toward an imaging-guided precision medicine. Radiol Med 2020;125(11):1013-1023.
11. von Knobelsdorff-Brenkenhoff F, Schulz-Menger J. Role of cardiovascular magnetic resonance in the guidelines of the European Society of Cardiology. J Cardiovasc Magn Reson 2016;18:6.
12. von Knobelsdorff-Brenkenhoff F, Pilz G, Schulz-Menger J. Representation of cardiovascular magnetic resonance in the AHA/ACC guidelines. J Cardiovasc Magn Reson 2017;19(1):70.
13. Qin C, Murali S, Lee E, et al. Sustainable low-field cardiovascular magnetic resonance in changing healthcare systems. Eur Heart J Cardiovasc Imaging 2022;23(6):e246-e260.
14. Centers for Medicare and Medicaid Services. Medicare Program: Hospital Outpatient Prospective Payment and Ambulatory Surgical Center Payment Systems and Quality Reporting Programs; Organ Acquisition; Rural Emergency Hospitals: Payment Policies, Conditions of Participation, Provider Enrollment, Physician Self-Referral; New Service Category for Hospital Outpatient Department Prior Authorization Process; Overall Hospital Quality Star Rating; COVID-19. 2023.
15. Simonetti OP, Ahmad R. Low-field cardiac magnetic resonance imaging: A compelling case for cardiac magnetic resonance's future. Circ Cardiovasc Imaging 2017;10(6):e005446.
16. Campbell-Washburn AE, Ramasawmy R, Restivo MC, et al. Opportunities in interventional and diagnostic imaging by using high-performance low-field-strength MRI. Radiology 2019;293:384-393.

17. Vosshenrich J, Breit HC, Bach M, Merkle EM. Economic aspects of low-field magnetic resonance imaging: Acquisition, installation, and maintenance costs of 0.55 T systems. Radiology 2022;62(5):400-404.

18. Bandettini WP, Shanbhag SM, Mancini C, et al. Evaluation of myocardial infarction by cardiovascular magnetic resonance at 0.55-T compared to 1.5-T. JACC Cardiovasc Imaging 2021;14(9):1866-1868.

19. Bandettini WP, Shanbhag SM, Mancini C, et al. A comparison of cine CMR imaging at 0.55 T and 1.5 T. J Cardiovasc Magn Reson 2020; 22(1):37.

20. Varghese J, Jin N, Giese D, et al. Building a comprehensive cardiovascular magnetic resonance exam on a commercial 0.55 T system: A pictorial essay on potential applications. Front Cardiovasc Med 2023;10:1120982.

21. Herfkens RJ, Higgins CB, Hricak H, et al. Nuclear magnetic resonance imaging of the cardiovascular system: Normal and pathologic findings. Radiology 1983;147(3):749-759.

22. Klein HM, Meyners W, Neeb B, Labenz J, Truümmler KH. Cardiac magnetic resonance imaging using an open 0.35 T system. J Comput Assist Tomogr 2007;31(3):430-434.

23. Takizawa M, Goto T, Mochizuki H, et al. Cardiac cine parallel imaging on a 0.7T open system. Magn Reson Med Sci 2004;3(1):45-49.

24. Hori M, Hagiwara A, Goto M, Wada A, Aoki S. Low-field magnetic resonance imaging: Its history and renaissance. Invest Radiol 2021; 56(11):669-679.

25. Klein HM. Low-field magnetic resonance imaging. Rofo 2020;192(6): 537-548.

26. Panting JR, Gatehouse PD, Yang GZ, et al. Echo-planar magnetic resonance myocardial perfusion imaging: Parametric map analysis and comparison with thallium SPECT. J Magn Reson Imaging 2001;13(2): 192-200.

27. Heatlie G, Pennell DJ. Cardiovascular magnetic resonance at 0.5T in five patients with permanent pacemakers. J Cardiovasc Magn Reson 2007;9(1):15-19.

28. Cheng CP, Herfkens RJ, Taylor CA, Feinstein JA. Proximal pulmonary artery blood flow characteristics in healthy subjects measured in an upright posture using MRI: The effects of exercise and age. J Magn Reson Imaging 2005;21(6):752-758.

29. Aoki S, Nanbu A, Araki T, et al. Active MR tracking on a 0.2 Tesla MR imager. Radiat Med 1999;17(3):251-257.

30. Guenthner C, Peereboom SM, Dillinger H, et al. Ramping down a clinical 3 T scanner: A journey into MRI and MRS at 0.75 T. Magma 2023. doi:10.1007/s10334-023-01089-9

31. SiemensHealthineers. Press release: MAGNETOM Free.Max. Volume 2022.

32. Fischer SE, Wickline SA, Lorenz CH. Novel real-time R-wave detection algorithm based on the vectorcardiogram for accurate gated magnetic resonance acquisitions. Magn Reson Med 1999;42(2):361-370.

33. Vishnevskiy V, Guenthner C, McGrath C, Kozerke S. Highly accelerated cardiac cine imaging on a lower-field 0.75T MRI. Proceedings of the ISMRM Annual Meeting; 2021. p. 0959.

34. Indik JH, Gimbel JR, Abe H, et al. 2017 HRS expert consensus statement on magnetic resonance imaging and radiation exposure in patients with cardiovascular implantable electronic devices. Heart Rhythm 2017;14(7):e97-e153.

35. Nazarian S, Hansford R, Rahsepar AA, et al. Safety of magnetic resonance imaging in patients with cardiac devices. N Engl J Med 2017; 377(26):2555-2564.

36. Russo RJ, Costa HS, Silva PD, et al. Assessing the risks associated with MRI in patients with a pacemaker or defibrillator. N Engl J Med 2017; 376(8):755-764.

37. Schwitter J, Gold MR, Al Fagih A, et al. Image quality of cardiac magnetic resonance imaging in patients with an implantable cardioverter defibrillator system designed for the magnetic resonance imaging environment. Circ Cardiovasc Imaging 2016;9(5):e004025.

38. Simonetti OP, Gross DC. Cardiovascular magnetic resonance in patients with magnetic resonance-conditional cardiac implantable electronic devices: What can we see? Circ Cardiovasc Imaging 2016; 9(5):e004970.

39. Schenck JF. The role of magnetic susceptibility in magnetic resonance imaging: MRI magnetic compatibility of the first and second kinds. Med Phys 1996;23(6):815-850.

40. Strach K, Naehle CP, Muhlsteffen A, et al. Low-field magnetic resonance imaging: Increased safety for pacemaker patients? Europace 2010;12(7):952-960.

41. Rusche T, Vosshenrich J, Winkel DJ, et al. More space, less noise-new-generation low-field magnetic resonance imaging systems can improve patient comfort: A prospective 0.55T-1.5T-scanner comparison. J Clin Med 2022;11(22):6705.

42. Dillinger H, Kozerke S, Guenthner C. Direct comparison of gradient Fidelity and acoustic noise of the same MRI system at 3 T and 0.75 T. Magn Reson Med 2022;88(4):1937-1947.

43. Bottomley PA, Foster TH, Argersinger RE, Pfeifer LM. A review of normal tissue hydrogen NMR relaxation times and relaxation mechanisms from 1-100 MHz: Dependence on tissue type, NMR frequency, temperature, species, excision, and age. Med Phys 1984;11(4):425-448.

44. Varghese J, Craft J, Crabtree CD, et al. Assessment of cardiac function, blood flow and myocardial tissue relaxation parameters at 0.35 T. NMR Biomed 2020;33:e4317.

45. Herzka DA, Ramasawmny R, Rogers T, et al. Estimating blood volume with ferumoxytol at 0.55 T. Proceedings of the ISMRM Annual Meeting; 2020. p. 1201.

46. Tian Y, Cui SX, Lim Y, Lee NG, Zhao Z, Nayak KS. Contrast-optimal simultaneous multi-slice bSSFP cine cardiac imaging at 0.55 T. Magn Reson Med 2023;89(2):746-755.

47. Reeder SB, Faranesh AZ, Boxerman JL, McVeigh ER. In vivo measurement of T*2 and field inhomogeneity maps in the human heart at 1.5 T. Magn Reson Med 1998;39(6):988-998.

48. Restivo MC, Ramasawmy R, Bandettini WP, Herzka DA, Campbell-Washburn AE. Efficient spiral in-out and EPI balanced steady-state free precession cine imaging using a high-performance 0.55T MRI. Magn Reson Med 2020;84(5):2364-2375.

49. Deng W, Stenger VA. A three-dimensional variable-density spiral spatial-spectral RF pulse with rotated gradients. Magn Reson Med 2010;63(3):828-834.

50. King KF, Ganin A, Zhou XJ, Bernstein MA. Concomitant gradient field effects in spiral scans. Magn Reson Med 1999;41(1):103-112.

51. Sica CT, Meyer CH. Concomitant gradient field effects in balanced steady-state free precession. Magn Reson Med 2007;57(4):721-730.

52. Hamilton JI, Truesdell W, Galizia M, Burris N, Agarwal P, Seiberlich N. A low-rank deep image prior reconstruction for free-breathing ungated spiral functional CMR at 0.55 T and 1.5 T. Magma 2023. doi: 10.1007/s10334-023-01088-w

53. Iglesias JE, Schleicher R, Laguna S, et al. Quantitative brain morphometry of portable low-field-strength MRI using super-resolution machine learning. Radiology 2023;306(3):e220522.

54. Xue H, Javed A, Ramasawmy R, Rehman A, Kellman P, Campbell-Washburn AE. CNNT denoising for cine imaging at 0.55T with higher acceleration rates. Proceedings from the 25th Annual SCMR Scientific Sessions; 2023.

55. Koonjoo N, Zhu B, Bagnall GC, Bhutto D, Rosen MS. Boosting the signal-to-noise of low-field MRI with deep learning image reconstruction. Sci Rep 2021;11(1):8248.

56. Global Cardiovascular Magnetic Resonance Registry (GCMR) Investigators, Kwong RY, Petersen SE, et al. The global cardiovascular magnetic resonance registry (GCMR) of the society for cardiovascular magnetic resonance (SCMR): Its goals, rationale, data infrastructure, and current developments. J Cardiovasc Magn Reson 2017;19(1):23.

57. Xue H, Inati S, Sørensen TS, Kellman P, Hansen MS. Distributed MRI reconstruction using gadgetron-based cloud computing. Magn Reson Med 2014;73:1015-1025.

58. Zu X, Varghese J, Simonetti O, Tao Q. AI analysis for low-field CMR: A head-to-head comparison of cine MRI at 0.35T, 1.5T, and 3.0T. Proceedings from the 24th Annual SCMR Scientific Sessions; 2022. p. 000077.

59. Rashid S, Han F, Gao Y, et al. Cardiac balanced steady-state free precession MRI at 0.35 T: A comparison study with 1.5 T. Quant Imaging Med Surg 2018;8(7):627-636.

60. Rehman A, Kellman P, Davies RH, et al. Convolutional neural network transformer (CNNT) for free-breathing real-time cine imaging. Artificial Intelligence in Cardiovascular Magnetic Resonance Imaging – A Joint Summit of the EACVI and SCMR; 2022.

61. Wang Z, Feng X, Mugler JP, Salerno M, Campbell-Washburn AE, Meyer CH. Spiral-in-out bSSFP real-time cine on a high performance 0.55T scanner. Proceedings of the ISMRM Annual Meeting; 2021. p. 0504.

62. Yagiz E, Garg P, Nayak K, Tian Y. Simultaneous multi-slice (SMS) real-time cardiac MRI at 0.55T. Proceedings from the 25th Annual SCMR Scientific Sessions; 2023.

63. Tian Y, Lee NG, Nayak KS. Realistic simulation of real-time cardiac cine and first pass perfusion on high performance 0.55T system. Proceedings of the ISMRM Annual Meeting; 2021. p. 2888.

64. Piccini D, Yerly J, Kober T, et al. Running free on a low-field: A proof of principle. Proceedings of the ISMRM Annual Meeting; 2021. p. 0747.

65. Bernstein MA, Zhou XJ, Polzin JA, et al. Concomitant gradient terms in phase contrast MR: Analysis and correction. Magn Reson Med 1998;39(2):300-308.

66. Shanbhag SM, Ramasawmy R, Bandettini WP, et al. Comparison of phase-contrast flow imaging at 0.55T and 1.5T. Proceedings of the ISMRM Annual Meeting; 2020. p. 2256.

67. Markl M, Pelc NJ. On flow effects in balanced steady-state free precession imaging: Pictorial description, parameter dependence, and clinical implications. J Magn Reson Imaging 2004;20(4):697-705.

68. Ramasawmy R, Herzka DA, Lederman RJ, Campbell-Washburn AE. Spiral bSSFP phase-contrast Flow at 0.55T. Proceedings of the ISMRM Annual Meeting; 2020. p. 1332.

69. Peper E, Dillinger H, McGrath C, Guenthner C, Kozerke S. Cine flow measurements using phase-contrast bSSFP at 0.75 Tesla. Proceedings of the ISMRM Annual Meeting; 2022. p. 0092.

70. Holtackers RJ, Van De Heyning CM, Chiribiri A, Wildberger JE, Botnar RM, Kooi ME. Dark-blood late gadolinium enhancement cardiovascular magnetic resonance for improved detection of subendocardial scar: review of current techniques. J Cardiovasc Magn Reson 2021;23(1):96.

71. Raeisi-Giglou P, Varghese J, Jin N, et al. Myocardial viability assessment with a novel 0.55T scanner compared to conventional 1.5T scanner. Proceedings from the 25th Annual SCMR Scientific Sessions; 2023.

72. Ding Y, Liu Y, Chen C, Jin N, Ahmad R, Simonetti O. Novel reconstruction method to improve sharpness of free-breathing cardiac MR late gadolinium enhancement images on a commercial 0.55T system. Proceedings from the 25th Annual SCMR Scientific Sessions; 2023.

73. Messroghli DR, Moon JC, Ferreira VM, et al. Clinical recommendations for cardiovascular magnetic resonance mapping of T1, T2, T2* and extracellular volume: A consensus statement by the Society for Cardiovascular Magnetic Resonance (SCMR) endorsed by the European Association for Cardiovascular Imaging (EACVI). J Cardiovasc Magn Reson 2017;19(1):75.

74. Mancini C, Bandettini WP, Kellman P, Xue H, Campbell-Washburn AE. Comparison of cardiac T1 mapping on a high-performance 0.55T scanner and a conventional 1.5T scanner. Proceedings of the ISMRT Annual Meeting; 2021. p. S31.

75. Crabb M, Kunze K, Munoz C, et al. 3D joint T1/T1rho mapping and water-fat imaging at 0.55T. Proceedings from the 25th Annual SCMR Scientific Sessions; 2023.

76. Varghese J, Nair N, Jin N, et al. T2 mapping in acute infarct characterization at 0.55 T. Proceedings from the 25th Annual SCMR Scientific Sessions; 2023.

77. Triadyaksa P, Oudkerk M, Sijens PE. Cardiac T(2) * mapping: Techniques and clinical applications. J Magn Reson Imaging 2020;52(5): 1340-1351.

78. Hernando D, Levin YS, Sirlin CB, Reeder SB. Quantification of liver iron with MRI: State of the art and remaining challenges. J Magn Reson Imaging 2014;40(5):1003-1021.

79. Campbell-Washburn AE, Mancini C, Conrey A, et al. Evaluation of hepatic iron overload using a contemporary 0.55 T MRI system. J Magn Reson Imaging 2021;55:1855-1863.

80. Ghugre NR, Doyle EK, Storey P, Wood JC. Relaxivity-iron calibration in hepatic iron overload: Predictions of a Monte Carlo model. Magn Reson Med 2015;74(3):879-883.

81. Farrelly C, Shah S, Davarpanah A, Keeling AN, Carr JC. ECG-gated multiecho Dixon fat-water separation in cardiac MRI: Advantages over conventional fat-saturated imaging. AJR Am J Roentgenol 2012; 199(1):W74-W83.

82. Chandarana H, Bagga B, Huang C, et al. Diagnostic abdominal MR imaging on a prototype low-field 0.55 T scanner operating at two different gradient strengths. Abdom Radiol (NY) 2021;46(12):5772-5780.

83. Franson D, Liu Y, Ramasawmy R, Campbell-Washburn A, Seiberlich N. Fat suppression using a rosette trajectory for low field magnetic resonance imaging. Proceedings of the ISMRM Annual Meeting; 2020. p. 0516.

84. Tian Y, Lim Y, Nayak KS. Real-time water fat imaging at 0.55T with spiral out-in-out-in sampling. Proceedings of the ISMRM Annual Meeting; 2022. p. 0516.

85. Castillo-Passi C, Crabb M, Munoz C, et al. Whole-heart cardiovascular magnetic resonance angiography (CMRA) with iNAVbased non-rigid motion-corrected reconstruction at 0.55T. Proceedings from the 25th Annual SCMR Scientific Sessions; 2023.

86. Kellman P, Hansen MS, Nielles-Vallespin S, et al. Myocardial perfusion cardiovascular magnetic resonance: Optimized dual sequence and reconstruction for quantification. J Cardiovasc Magn Reson 2017; 19(1):43.

87. Korosoglou G, Giusca S, Hofmann NP, et al. Strain-encoded magnetic resonance: A method for the assessment of myocardial deformation. ESC Heart Fail 2019;6(4):584-602.

88. Erley J, Zieschang V, Lapinskas T, et al. A multi-vendor, multi-center study on reproducibility and comparability of fast strain-encoded cardiovascular magnetic resonance imaging. Int J Cardiovasc Imaging 2020;36(5):899-911.

89. Liu Y, Tani D, Joseph M, et al. Feasibility of strain encoded (SENC) MRI to assess cardiac contractility on a commercial 0.55T system. Proceedings of the ISMRM Annual Meeting; 2023.

90. Liu Y, Osman N, Fleischman S, Simonetti O. Feasibility of Strain Encoded MRI (SENC) on a commercial 0.55T system. Proceedings from the 25th Annual SCMR Scientific Sessions; 2023.

91. Rogers T, Ratnayaka K, Khan JM, et al. CMR fluoroscopy right heart catheterization for cardiac output and pulmonary vascular resistance: Results in 102 patients. J Cardiovasc Magn Reson 2017;19(1):54.

92. Ratnayaka K, Kanter JP, Faranesh AZ, et al. Radiation-free CMR diagnostic heart catheterization in children. J Cardiovasc Magn Reson 2017;19(1):65.

93. Knight DS, Kotecha T, Martinez-Naharro A, et al. Cardiovascular magnetic resonance-guided right heart catheterization in a conventional CMR environment – predictors of procedure success and duration in pulmonary artery hypertension. J Cardiovasc Magn Reson 2019;21(1):57.

94. Pushparajah K, Tzifa A, Razavi R. Cardiac MRI catheterization: A 10-year single institution experience and review. Interv Cardiol 2014; 6(3):335-346.

95. Veeram Reddy SR, Arar Y, Zahr RA, et al. Invasive cardiovascular magnetic resonance (iCMR) for diagnostic right and left heart catheterization using an MR-conditional guidewire and passive visualization in congenital heart disease. J Cardiovasc Magn Reson 2020;22(1):20.

96. Pandya B, Quail MA, Steeden JA, et al. Real-time magnetic resonance assessment of septal curvature accurately tracks acute hemodynamic changes in pediatric pulmonary hypertension. Circ Cardiovasc Imaging 2014;7(4):706-713.

97. Chubb H, Harrison JL, Weiss S, et al. Development, preclinical validation, and clinical translation of a cardiac magnetic resonance – electrophysiology system with active catheter tracking for ablation of cardiac arrhythmia. JACC Clin Electrophysiol 2017;3(2):89-103.

98. Hilbert S, Sommer P, Gutberlet M, et al. Real-time magnetic resonance-guided ablation of typical right atrial flutter using a combination of active catheter tracking and passive catheter visualization in man: Initial results from a consecutive patient series. Europace 2016; 18(4):572-577.

99. Paetsch I, Sommer P, Jahnke C, et al. Clinical workflow and applicability of electrophysiological cardiovascular magnetic resonance-guided radiofrequency ablation of isthmus-dependent atrial flutter. Eur Heart J Cardiovasc Imaging 2019;20(2):147-156.

100. Rogers T, Mahapatra S, Kim S, et al. Transcatheter myocardial needle chemoablation during real-time magnetic resonance imaging: A new approach to ablation therapy for rhythm disorders. Circ Arrhythm Electrophysiol 2016;9(4):e003926.

101. Rogers T, Ratnayaka K, Karmarkar P, et al. Real-time magnetic resonance imaging guidance improves the diagnostic yield of endomyocardial biopsy. JACC Basic Transl Sci 2016;1(5):376-383.

102. Ratnayaka K, Rogers T, Schenke WH, et al. Magnetic resonance imaging-guided transcatheter cavopulmonary shunt. JACC Cardiovasc Interv 2016;9(9):959-970.

103. Mukherjee RK, Roujol S, Chubb H, et al. Epicardial electroanatomical mapping, radiofrequency ablation, and lesion imaging in the porcine left ventricle under real-time magnetic resonance imaging guidance-an in vivo feasibility study. Europace 2018;20(FI2):f254-f262.

104. Ozen AC, Russe MF, Lottner T, et al. RF-induced heating of interventional devices at 23.66 MHz. Magma 2023. doi:10.1007/s10334-023-01099-7

105. Kolandaivelu A, Bruce CG, Ramasawmy R, et al. Native contrast visualization and tissue characterization of myocardial radiofrequency ablation and acetic acid chemoablation lesions at 0.55 T. J Cardiovasc Magn Reson 2021;23(1):50.

106. Lardo AC, McVeigh ER, Jumrussirikul P, et al. Visualization and temporal/spatial characterization of cardiac radiofrequency ablation lesions using magnetic resonance imaging. Circulation 2000; 102(6):698-705.

107. Seemann F, Bruce CG, Khan JM, et al. Dynamic pressure-volume loop analysis by simultaneous real-time cardiovascular magnetic resonance and left heart catheterization. J Cardiovasc Magn Reson 2023;25(1):1.

108. Basar B, Sonmez M, Yildirim DK, et al. Susceptibility artifacts from metallic markers and cardiac catheterization devices on a high-performance 0.55 T MRI system. Magn Reson Imaging 2021;77:14-20.

109. Basar B, Bruce CG, Herzka DA, Lederman RJ, Campbell-Washburn A. Computer vision segmentation of nitinol guidewires during MRI-guided cardiovascular catheterizations. Proceedings from the 23rd Annual SCMR Scientific Sessions; 2020. p. 751432.

110. Basar B, Bruce CG, Jaimes A, et al. Amplification of imaging signature from off-the-shelf nitinol guidewires during MRI guided catheterization using a U-Net. Proceedings from the 24th Annual SCMR Scientific Sessions; 2022. p. 000298.

111. Yildirim DK, Uzun D, Bruce CG, et al. An interventional MRI guidewire combining profile and tip conspicuity for catheterization at 0.55T. Magn Reson Med 2023;89(2):845-858.

112. Yildirim DK, Bruce C, Uzun D, et al. A 20-gauge active needle design with thin-film printed circuitry for interventional MRI at 0.55T. Magn Reson Med 2021;86(3):1786-1801.

113. Armstrong A, Krishnamurthy R, Swinning J, et al. Feasibility of MRI-guided cardiac catheterization, angioplasty, and stenting in a 0.55T scanner with limited gradient performance. Proceedings from the 25th Annual SCMR Scientific Sessions; 2023.

114. Mooiweer R, Rogers C, Neji R, Razavi R, Roujol S. Characterization of cardiac PRFS thermometry at 0.55T. Proceedings from the 25th Annual SCMR Scientific Sessions; 2023.

115. Mayinger M, Kovacs B, Tanadini-Lang S, et al. First magnetic resonance imaging-guided cardiac radioablation of sustained ventricular tachycardia. Radiother Oncol 2020;152:203-207.

116. Akdag O, Borman PTS, Woodhead P, et al. First experimental exploration of real-time cardiorespiratory motion management for future stereotactic arrhythmia radioablation treatments on the MR-linac. Phys Med Biol 2022;67(6):065003.

117. Bhattacharya I, Ramasawmy R, Javed A, et al. Oxygen-enhanced functional lung imaging using a contemporary 0.55 T MRI system. NMR Biomed 2021;34:e4562.

118. Campbell-Washburn AE. 2019 ATS BEAR cage winning proposal: Lung imaging using high-performance low-field MRI. Am J Respir Crit Care Med 2020;201:1333-1336.

119. Campbell-Washburn AE, Malayeri AA, Jones EC, et al. T2-weighted lung imaging using a 0.55-T MRI system. Radiology: Cardiothoracic Imaging 2021;3(3):e200611.

120. Javed A, Ramasawmy R, O'Brien K, et al. Self-gated 3D stack-of-spirals UTE pulmonary imaging at 0.55T. Magn Reson Med 2022; 87(4):1784-1798.

121. Bhattacharya I, Ramasawmy R, Javed A, et al. Assessment of lung structure and regional function using 0.55 T MRI in patients with lymphangioleiomyomatosis. Invest Radiol 2022;57(3):178-186.

122. Heiss R, Tan L, Schmidt S, et al. Pulmonary dysfunction after pediatric COVID-19. Radiology 2023;306(3):e221250.

123. Levy S, Heiss R, Grimm R, et al. Free-breathing low-field MRI of the lungs detects functional alterations associated with persistent symptoms after COVID-19 infection. Invest Radiol 2022;57(11): 742-751.

124. Klaar R, Rabe M, Gaass T, et al. Ventilation and perfusion MRI at a 0.35 T MR-Linac: Feasibility and reproducibility study. Radiat Oncol 2023;18(1):58.

125. Seemann F, Javed A, Chae R, et al. Imaging gravity-induced lung water redistribution with automated inline processing at 0.55 T cardiovascular magnetic resonance. J Cardiovasc Magn Reson 2022;24(1):35.

126. Seemann F, Javed A, Khan JM, et al. Dynamic lung water magnetic resonance imaging during exercise. Magn Reson Med, 2023; doi:10.1002/mrm.29716 (online ahead of print).

127. Bandettini WP, Mancini C, Shanbhag SM, et al. A comparison of metal artifacts in cardiovascular MRI at 0.55T and 1.5T. Proceedings of the ISMRM Annual Meeting; 2021. p. 3636.

128. Keskin K, Hargreaves BA, Nayak KS. Imaging near metal at 0.55 T using gradient-echo based sequences: Feasibility and opportunities. Proceedings of the ISMRM Annual Meeting; 2022. p. 0957.

129. Van Speybroeck CDE, O'Reilly T, Teeuwisse W, Arnold PM, Webb AG. Characterization of displacement forces and image artifacts in the presence of passive medical implants in low-field (<100 mT) permanent magnet-based MRI systems, and comparisons with clinical MRI systems. Phys Med 2021;84:116-124.

130. Gilk T, Kanal E. MRI safety considerations associated with low-field MRI: Mostly good news. Magma 2023. doi:10.1007/s10334-023-01079-x

131. Krainak DM, Zeng R, Li N, Woods TO, Delfino JG. US regulatory considerations for low field magnetic resonance imaging systems. Magma 2023. doi:10.1007/s10334-023-01083-1

132. Carucci LR. Imaging obese patients: Problems and solutions. Abdom Imaging 2013;38(4):630-646.

133. Uppot RN. Technical challenges of imaging & image-guided interventions in obese patients. Br J Radiol 2018;91(1089):20170931.

134. Budzynska A, Osiecki S, Mazurek A, Piszczek S, Dziuk M. Feasibility of myocardial perfusion imaging studies in morbidly obese patients with a cadmium-zinc-telluride cardiac camera. Nucl Med Rev Cent East Eur 2019;22(1):18-22.

135. Fursevich DM, LiMarzi GM, O'Dell MC, Hernandez MA, Sensakovic WF. Bariatric CT imaging: Challenges and solutions. Radiographics 2016;36(4):1076-1086.

136. Israel GM, Cicchiello L, Brink J, Huda W. Patient size and radiation exposure in thoracic, pelvic, and abdominal CT examinations performed with automatic exposure control. AJR Am J Roentgenol 2010; 195(6):1342-1346.

137. Huo D, Rill L. Hallway conversations in physics(what is the relative radiation dose increase for an obese patient undergoing radiography, fluoroscopy, and CT examinations?). AJR Am J Roentgenol 2017; 208(2):W56-W57.

138. Uppot RN. Impact of obesity on radiology. Radiol Clin North Am 2007;45(2):231-246.

139. Uppot RN, Sahani DV, Hahn PF, Gervais D, Mueller PR. Impact of obesity on medical imaging and image-guided intervention. AJR Am J Roentgenol 2007;188(2):433-440.

140. Dempsey MF, Condon B. Thermal injuries associated with MRI. Clin Radiol 2001;56(6):457-465.

141. Durbridge G. Magnetic resonance imaging: Fundamental safety issues. J Orthop Sports Phys Ther 2011;41(11):820-828.

142. Eisenstein I, Edelstein J, Sarma R, Sanmarco M, Selvester RH. The electrocardiogram in obesity. J Electrocardiol 1982;15(2):115-118.

143. Constantine G, Shan K, Flamm SD, Sivananthan MU. Role of MRI in clinical cardiology. Lancet 2004;363(9427):2162-2171.

144. Salerno M, Sharif B, Arheden H, et al. Recent advances in cardiovascular magnetic resonance: Techniques and applications. Circ Cardiovasc Imaging 2017;10(6):e003951.

145. Doeblin P, Kelle S. Cardiac magnetic resonance imaging: The echo of the obese? Eur Heart J Cardiovasc Imaging 2021;22(5):528-529.

146. Ge Y, Steel K, Antiochos P, et al. Stress CMR in patients with obesity: Insights from the stress CMR perfusion imaging in the United States (SPINS) registry. Eur Heart J Cardiovasc Imaging 2021;22(5):518-527.

147. Shah RV, Heydari B, Coelho-Filho O, et al. Vasodilator stress perfusion CMR imaging is feasible and prognostic in obese patients. JACC Cardiovasc Imaging 2014;7(5):462-472.

148. Simonetti OP, Varghese J, Jin N, et al. Cardiac MRI on the MAGNETOM Free.Max: The Ohio state experience. MAGNETOM Flash 2023;83(1):33-43.

149. Hutter J, Verdera JA, Tomi-Tricot R, et al. Fetal low field MRI – The first 150 cases. MAGNETOM Flash 2023;84(2):78-84.

150. Tian Y, Detterich J, John Wood M, Joshi AA, Pruetz JD, Nayak K. Real-time fetal cardiac MRI at 0.55T enables assessment of ventricular function and heart and great vessel anatomy. Proceedings from the 25th Annual SCMR Scientific Sessions; 2023.

151. Goolaub D, Tian Y, Amerom Jv, et al. Multiresolution comparison of fetal CINE MRI at 0.55T. Proceedings of the ISMRM Annual Meeting; 2023.

152. Amerom Fv, Tian Y, Goolaub D, et al. Fetal cardiac 3D CINE MRI at low field – whole heart slice-to-volume reconstruction from real-time spiral SSFP at 0.55T. Proceedings of the ISMRM Annual Meeting; 2023.

153. Bustin A, Rashid I, Cruz G, et al. 3D whole-heart isotropic sub-millimeter resolution coronary magnetic resonance angiography with non-rigid motion-compensated PROST. J Cardiovasc Magn Reson 2020;22(1):24.

154. Hamilton JI, Jiang Y, Chen Y, et al. MR fingerprinting for rapid quantification of myocardial T1, T2, and proton spin density. Magn Reson Med 2017;77(4):1446-1458.

155. Christodoulou AG, Shaw JL, Nguyen C, et al. Magnetic resonance multitasking for motion-resolved quantitative cardiovascular imaging. Nat Biomed Eng 2018;2(4):215-226.

156. Sarracanie M. Fast quantitative low-field magnetic resonance imaging with OPTIMUM-optimized magnetic resonance fingerprinting using a stationary steady-state Cartesian approach and accelerated acquisition schedules. Invest Radiol 2022;57(4):263-271.

157. Campbell-Washburn AE, Jiang Y, Korzdorfer G, Nittka M, Griswold MA. Feasibility of MR fingerprinting using a high-performance 0.55 T MRI system. Magn Reson Imaging 2021;81:88-93.

158. Sarracanie M, Cohen O, Rosen MS. 3D balanced-EPI magnetic resonance fingerprinting at 6.5 mT. Proceedings of the 23rd Annual Meeting of the International Society for Magnetic Resonance in Medicine; 2015. p. 3385.

159. Liu Y, Hamilton J, Jiang Y, Seiberlich N. Assessment of MRF for simultaneous T(1) and T(2) quantification and water-fat separation in the liver at 0.55 T. Magma 2022. doi:10.1007/s10334-022-01057-9

160. Nikpanah M, Willoughby W, Campbell-Washburn A, et al. Low versus ultra-high field MRI: How to select your MRI fleet. Appl Radiol 2023; 52(1):28-41.

161. Kober F, Jao T, Troalen T, Nayak KS. Myocardial arterial spin labeling. J Cardiovasc Magn Reson 2016;18:22.

162. Tsaftaris SA, Zhou X, Tang R, Li D, Dharmakumar R. Detecting myocardial ischemia at rest with cardiac phase-resolved blood oxygen level-dependent cardiovascular magnetic resonance. Circ Cardiovasc Imaging 2013;6(2):311-319.

163. Lee NG, Ramasawmy R, Lim Y, Campbell-Washburn AE, Nayak KS. MaxGIRF: Image reconstruction incorporating concomitant field and gradient impulse response function effects. Magn Reson Med 2022; 88(2):691-710.

164. Ramasawmy R, Mugler III JP, Javed A, et al. Concomitant Field Compensation of Spiral Turbo Spin-Echo at 0.55T. MAGMA 2023; doi:10.1007/s10334-023-01103-0 (online ahead of print).

165. Wang Z, Feng X, Ramasawmy R, Campbell-Washburn AE, JP Mugler III, Meyer CH. Maxwell field compensation for 2D spiral-ring turbo spin-echo imaging at 0.55T and 1.5T. Proceedings of the ISMRM Annual Meeting; 2022. p. 0319.